LEIDEN UNIVERSITY

BACHELOR THESIS

Observation of Biphoton Speckle from Random Phase Plates

Author:
J.J.D (Hans) MOERMAN

Supervisors:
Ir. Wouter H. PEETERS
Dr. Martin P. VAN EXTER

October 9, 2008

Abstract

We present the first measurements of two-photon speckle patterns. Spatially entangled two-photon states are scattered from a random phase plate (diffuser) and a random two-photon interference pattern is formed in the far field of the diffuser. The two-photon speckle pattern has been observed by measuring the coincidence count rate as a function of the transverse positions of two single-photon detectors. The 'ordinary' intensity speckle that would have been observed under coherent illumination is absent as the incident light is incoherent at the one-photon level. The photon pairs are produced via the nonlinear optical process of spontaneous parametric down-conversion in a periodically-poled $KTiOPO_4$ crystal (PPKTP).

To fully understand biphoton speckle we first thoroughly researched the properties of the diffusers for single photon speckle. We found that the far field intensity distributions and the average intensity profile were close to theory. Contrary to expectations we found that all diffusers were slightly anisotropic, having two different scattering angles. We found that the light shaping diffusers show signs of birefringence. It depends on the diffuser how strong this birefringence is and how much variation there is on the birefringence. The orientations of the fast and the slow axis are constant over the surface of the diffuser.

Acknowledgements

When I first met Wouter Peeters he was very eager to show me single photon speckles. I liked the combination of optics and statistics involved. He promised we would be the first people ever to see a biphoton speckle pattern. That was four months ago. Now I can present this bachelors thesis with theory and measurements of biphoton speckle.

During the project Wouter has been a great support. I would like to thank him both for his enthusiasm and his support with my experiments and the writing of the thesis. I would like to thank Martin van Exter for helping me with the theoretical background.

Also I would like to thank the other members of the Quantum Optics and Quantum Information group for their support with my experiments and the discussions at the coffee table.

J.J.D (HANS) MOERMAN

Leiden
October 9, 2008

Contents

1 Introduction

Speckle is a random intensity pattern that is caused by the interference of many random, but coherent field contributions [**?**]. Although speckles have been known since Newton, speckle research flourished in the 70s when the first speckle pictures were made by illuminating rough surfaces with laser light [**?**].

At first these speckles were considered a major drawback to research fields such as holography, because the images are generally very grainy. Later the applications of speckles were discovered. The speckle images often contained very interesting information on the surface where the light last scattered. Speckle imaging is nowadays used in astronomy [**?**][**?**] and biology [**?**].

Much has been written on speckle patterns with coherent illumination using laser light, we will refer to this as classical speckles [**?**]. In this thesis we will shed another light on speckles. We will generate speckles that do not manifest themselves in the intensity but are observed only in the coincidences of photon detections at two spatially separated detectors. We will show that although the classical speckles are not present we can detect a speckle pattern of a higher order, a speckle pattern that is present in non local correlations, biphoton speckle.

Biphoton speckle is generated by illuminating a random phase plate (diffuser) with light generated with the nonlinear optical process of spontaneous parametric down-conversion (SPDC). SPDC is a process in quantum optics where a high-energy photon (blue) is converted to two low-energy photons (infrared). Because of energy and momentum conservation laws the infrared photons contain information about the original blue photon [**?**]. We say that the photons are entangled. Before detection there is a fundamental uncertainty in the position and momentum of the entangled photons. Detection of the momentum of one of the photons yields information about the momentum of the other photon. The uncertainty in momentum of the second photon is resolved instantaneously. Because the photons are spatially separated this would imply seemingly superluminescent communication between the particles. For a discussion see the original article on the EPR-paradox [**?**] or review by Bell [**?**].

The far field of the random phase plate will be measured by two detectors that can count single photons. If two photons enter detector 1 and detector 2 simultaneously we will speak of a coincidence. We will show the presence of biphoton speckle in the coincidence counts, under conditions where single photon speckle in the intensities (or single photon counts) is absent.

This thesis comprises of two main parts. The first part consists of chapters 2 to 4.

Here we will outline the theory for the classical intensity speckles and provide speckle statistics for three types of random phase plates. These speckles are generated using a coherent source. In this part we will also look into the birefringent behavior of these diffusers. Through this parts we will build up a thorough knowledge on the behavior of the diffusors on the single photon level.

The second part, consisting of chapters 5 to 7, is devoted to the biphoton speckle. The diffuser is illuminated with photon pairs resulting from the SPDC process. Using another setup we will generate the first measurements of biphoton speckle. In this measurement the single photon speckle in intensity is no longer visible but there is still speckle in the coincidences. Biphoton speckle is fundamentally different from single photon speckle because the interference depends on the transversal coordinates of both detectors. A single biphoton speckle thus depends on four coordinates. We used different scanning techniques to visualize the biphoton speckle. The size of the speckles we measured is in accordance with our theory.

2 Theory classical speckle

We will start the theory of the classical speckle with a description of the electromagnetic field. We will make a pump spot on the diffuser plate by focussing a linearly polarized Gaussian beam. A mode is a stationary solution to the Maxwell equations and can be characterized by the electric field vector $\boldsymbol{E}(\boldsymbol{r})$ at position $\boldsymbol{r}$. In the focus of the beam there is no curvature and we can describe the beam by a plane wave front. We will assume that the light is travelling in the z-direction, and therefore the electric field has an x and a y-component. The electric field is a complex vector where the absolute value corresponds to the amplitude and the phase is the phase of the field. The transverse profile of the pump at the diffuser is Gaussian and can be described by the formula [**?**]

$$\boldsymbol{E}_0(\boldsymbol{x}) = \boldsymbol{E}_0 \exp\left(-\frac{\boldsymbol{x}^2}{w_0^2}\right), \tag{1}$$

where w_0 is called the width of the beam, $\boldsymbol{E}_0$ is the maximum field strength and $\boldsymbol{x}$ contains the transverse positions x and y on the diffuser. The intensity is a real and positive number and is defined as the squared absolute value of the electric field

$$I \sim |\boldsymbol{E}|^2, \tag{2}$$

and so the intensity of the pump is easily calculated

$$I_0(\boldsymbol{x}) = I_0 \exp\left(-2\frac{\boldsymbol{x}^2}{w_0^2}\right), \tag{3}$$

where $I_0 = |\boldsymbol{E}_0|^2$ is the peak intensity. Please note the presence of an extra factor 2 in the exponent. The random phase plate can completely be characterized by a random function $\phi(\boldsymbol{x})$. The form of this function depends on the position of the pump spot on the diffuser. The diffuser will not change the amplitude of the field, but can add a random phase. Based on this function we can give the formula for the field directly after the diffuser plate

$$\boldsymbol{E}_d(\boldsymbol{x}) = \boldsymbol{E}_0(\boldsymbol{x}) \exp\left[i\boldsymbol{\phi}(\boldsymbol{x})\right]. \tag{4}$$

Using a Fourier transform we can propagate this near field to the far field [**?**][**?**] and find its dependence on the angle $\boldsymbol{\theta}$. This Fourier transform has form

$$\boldsymbol{E}_{\mathrm{FF}}(\boldsymbol{\theta}) = \int \boldsymbol{E}_d(\boldsymbol{x}') \exp\left(\frac{-2i\pi\boldsymbol{\theta}\cdot\boldsymbol{x}'}{\lambda_0}\right) d\boldsymbol{x}', \tag{5}$$

where λ_0 is the wavelength of the pump beam. We find that if the pump spot is sufficiently large compared to the structures on the diffuser plate that the average intensity in the far field should be Gaussian[1]

$$\langle I_{\text{FF}}(\boldsymbol{\theta})\rangle_D = I_0 \exp\left(-2\boldsymbol{\theta}^T \mathcal{Q}^{-1}\boldsymbol{\theta}\right). \tag{6}$$

The operation $\langle\cdot\rangle_D$, takes the expectation value of a certain function over all possible positions of the pump spot on the diffuser. Here the matrix $\mathcal{Q}$ contains the widths of the diffuser in the x and the y-direction. Generally the scattering of the diffuser will on average have a elliptical shape. If the x and y are aligned with the long axis of this ellipse then $\mathcal{Q}$ is a diagonal matrix,

$$\mathcal{Q} = \begin{pmatrix} \theta_x^2 & 0 \\ 0 & \theta_y^2 \end{pmatrix}. \tag{7}$$

where θ_x and θ_y are the opening angles in the two directions of the diffuser.

Dependencies of second order in the speckles are described by the autocorrelation function

$$g^{(2)}(\boldsymbol{\Delta\theta}) \equiv \frac{\langle I_{\text{FF}}(\boldsymbol{\theta})\, I_{\text{FF}}(\boldsymbol{\theta}-\boldsymbol{\Delta\theta})\rangle_{XY}}{\langle I_{\text{FF}}(\boldsymbol{\theta})\rangle_{XY}^2}. \tag{8}$$

For a single speckle pattern it is defined as the product of an intensity and a second intensity at a displacement, scaled with the average intensity squared. The operator $\langle\cdot\rangle_{XY} = \int_{\text{Picture}} \cdot dxdy$ takes the spatially averaged value of the function within brackets over a single speckle image. If the angular dependence is depicted, for example $I(\boldsymbol{\theta})$, we integrate over angles θ_x and θ_y.

When we average this value over many positions of the diffuser we expect[2] to find the average correlation function. We expect this function to have a double Gaussian profile

$$\left\langle g^{(2)}(\boldsymbol{\Delta\theta})\right\rangle_D \sim \left[\exp\left(-\boldsymbol{\Delta\theta}^T \mathcal{Q}^{-1}\boldsymbol{\Delta\theta}\right) + \exp\left(-\left(\frac{\pi w_0 \boldsymbol{\Delta\theta}}{\lambda_0}\right)^2\right)\right]. \tag{9}$$

The first term is called the shell function and corresponds to the coherence within the angular spread of the diffuser. It is parameterized by the matrix $\mathcal{Q}$. The second term, the spike function, corresponds to the correlation generated by the individual speckles. The size of the speckles is inversely proportional to the size of the pump spot w_0.

[1] A detailed derivation can be found in Section B. Although the notation is somewhat different for clarity reasons.

[2] A derivation can be found in Appendix Section B

We will now define the number of channels for random media analogous to the definition of the optical etendue

$$N_c \equiv \frac{\int \widehat{I_0}(\boldsymbol{x}')d\boldsymbol{x}' \int \left\langle \widehat{I_{\mathrm{FF}}}(\boldsymbol{\theta}') \right\rangle_D d\boldsymbol{\theta}'}{\lambda_0^2}. \tag{10}$$

The hat operator $\widehat{\cdot}$ scales the intensity with the maximum intensity. In the far field the intensity is scaled with the maximum average intensity. For a diffuser plate the number of channels depends on the width of the shell over the width of the spike

$$N_c = \frac{\pi^2 w_0^2 \theta_x \theta_y}{\lambda_0^2}. \tag{11}$$

The far field intensities result from many uncorrelated field contributions with random phases. We expect[3] the intensities in the far field to have an exponential distribution with the average intensity from Equation (6). The distribution function for the intensity I at position $\boldsymbol{\theta}$ is given by

$$P_I(I, \boldsymbol{\theta}) = \frac{1}{\langle I(\boldsymbol{\theta}) \rangle_D} \exp\left(\frac{-I}{\langle I(\boldsymbol{\theta}) \rangle_D} \right). \tag{12}$$

The distribution depends explicitly on the angle $\boldsymbol{\theta}$. To be able to compute statistics based on one speckle pattern we define a scaled intensity with a distribution that has no $\boldsymbol{\theta}$ dependence. We scale the intensities with the average intensity

$$\bar{I}(\boldsymbol{\theta}) = \frac{I(\boldsymbol{\theta})}{\langle I(\boldsymbol{\theta}) \rangle_D}, \tag{13}$$

to obtain the scaled intensity. The distribution for the scaled intensity is

$$P_{\bar{I}}(\bar{I}) = \exp(-\bar{I}). \tag{14}$$

For the exponential distribution of Equation (14) the expectation of the squared intensity is twice that of the intensity squared.

$$\left\langle \bar{I}^2 \right\rangle_{XY} = 2 \left\langle \bar{I} \right\rangle_{XY}^2 \tag{15}$$

The contrast of a speckle pattern is defined as

$$C \equiv \frac{\sqrt{\left\langle \bar{I}^2 \right\rangle_{XY} - \left\langle \bar{I} \right\rangle_{XY}^2}}{\left\langle \bar{I} \right\rangle_{XY}} \tag{16}$$

and has a value of 1 for an exponential distribution of $\bar{I}$. Speckle with a contrast of $C = 1$ is called a fully developed speckle.

[3] A derivation is in Section A.

3 Setup classical speckle

A schematic picture of the experimental setup is given in Figure 1. We use a Coherent Verdi Laser to pump a + titanium-sapphire, laser. This Coherent 899 Ring laser, emits a beam in the infrared range (the wavelength $\lambda_0 = 826$ nm). This beam is led through a Faraday isolator and a half wave plate followed by a polarizer, to modify the intensity of the beam. Using lens A this beam is then focussed into a single mode fiber (with a mode field diameter of MFD $= 5.6$ μm) to obtain a transverse Gaussian profile. The importance of using single mode fibers is stressed, since in multi mode fibers the speckles that will show up can be an artifact of the fiber rather than the diffuser plate. The light exiting the fiber is focussed onto a diffuser plate using an objective lens B ($f = 10$ mm). The pump beam is normally incident on the rough surface of the diffuser and exits the diffuser at the opposite planar surface. The distance between the lens used for focussing and the plate is about 1 m. This results in a focus of width of $w_0 = 230$ μm. The beam has a Gaussian beam profile, the intensity as function the transverse direction is given by Equation (1).

The beam is redirected twice using mirrors. Between the lens and the diffuser is a polarizer that transmits in the vertical polarization. The verticality of the polarization is checked in a system of two polarizers, where a polarizer in vertical and horizontal direction are blocking all light. Turning one of the polarizers $180\,^\circ$ also yields a blockade of all light only if the polarizers are exactly horizontally and vertically aligned.

Directly behind the diffuser is another polarizer to control for the polarizations exiting the diffuser. The transmission of this second polarizer is about 95% at the relevant wavelength. If this polarizer also has the vertical polarization direction we shall refer to the setup as parallel polarized. If the polarization is horizontal the setup is cross polarized. If the polarizer is removed we shall refer to the situation as mixed.

3.1 Imaging system for the near field (CCD1)

Behind the diffuser are two imaging systems. The first system produces a magnified image of the near field using a telescope. The first lens has a focal distance of $f_1 = 100$ mm and the second lens has a focal distance of $f_2 = 300$ mm. Using the autocollimation procedure (Appendix D) the second lens is aligned so that the CCD camera is in the focus of the second lens, the distance between this lens and the camera is $f_2 = 300$ mm. The distance between the first lens and the second lens is approximately $f_1 + f_2 = 400$ mm, however the exact alignment of this lens depends on the other CCD camera position (the detailed procedure is given in the next section). The diffuser is placed perfectly in the focal point of the first lens. To achieve this we first replace the diffuser with an object

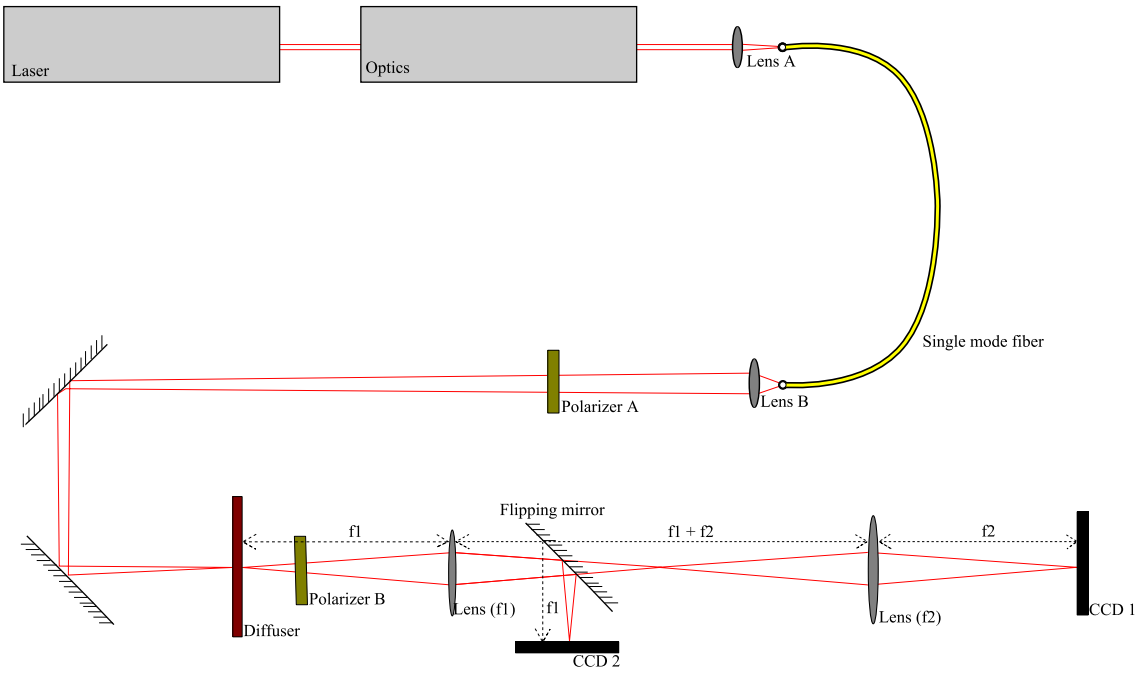

Figure 1: Schematic picture of the experimental setup for the classical speckle experiment. A beam from the laser is guided through a Faraday isolator before being focussed into a single mode fiber. From the single mode fiber the beam again is focussed onto a diffuser plate. The distance between the diffuser plate and the lens is approximately 1m. Light is led through a polarizer so the beam has a vertical polarization. Behind the diffuser two imaging systems are used to make near field and far field images of the plate. These systems are separated using a flipping mirror. Using a telescope system with two lenses (focal distance f1 and f2) a near field of the diffuser is made. And using the same lens with focal distance f1 a far field image is made in a f-f system. Both imaging systems contain a second polarizer directly after the diffuser.

	Opening angle	Manufacturer	Owner	Orientation angle
Diffuser 1	$0.5°$	Physical Optics Corporation	Martin	$333°$
Diffuser 2	$0.5°$	Physical Optics Corporation	Eric	$154°$
Diffuser 3	$1°$	Physical Optics Corporation	Eric	$15°$

Table 1: Details of the diffuser plates used in the classical speckle measurements. The stated opening angle is provided by the manufacturer. The orientation angle (A) gives information about the orientation of the diffuser in the rotator mount. Details about its definition can be found in Figure 2

(USAF plate, Appendix D) and adjust the position of the diffuser/USAF plate to give a perfect image of the USAF plate in the near field.

The near field telescope system results in a magnification of $f_2/f_1 = 3$. The width of the image of the pump beam therefore is approximately 600 μm The size of the CCD camera (Apogee Alta) is 512×768 pixels of 9 μm $\times$ 9 μm.

3.2 Imaging system for the far field (CCD2)

The far field image is made using an $f_1 - f_1$ imaging system. Using a mirror the beam is deflected after the first lens into the second CCD camera. The lens is aligned using the autocollimation method so that the camera is exactly in the focus of the lens. In the near field alignment care is taken so that the diffuser is in the focus of the lens. With diffusers of $0.5\,°$ we expect the pictures on the CCD camera to have a width of 100 mm $\left(\frac{0.5\,°}{180\,°/\pi}\right) =$ 1.7 mm. The size of the CCD camera (Apogee Alta) is 512×768 pixels of 9 μm $\times$ 9 μm.

3.3 Diffusers

In this experiment we used three different diffuser plates. They are labelled diffuser 1 through 3. Their properties are listed in Table 1. The diffusers are placed in rotator mounts. A clarification of the positioning of the diffuser in these mounts is given in Figure 2.

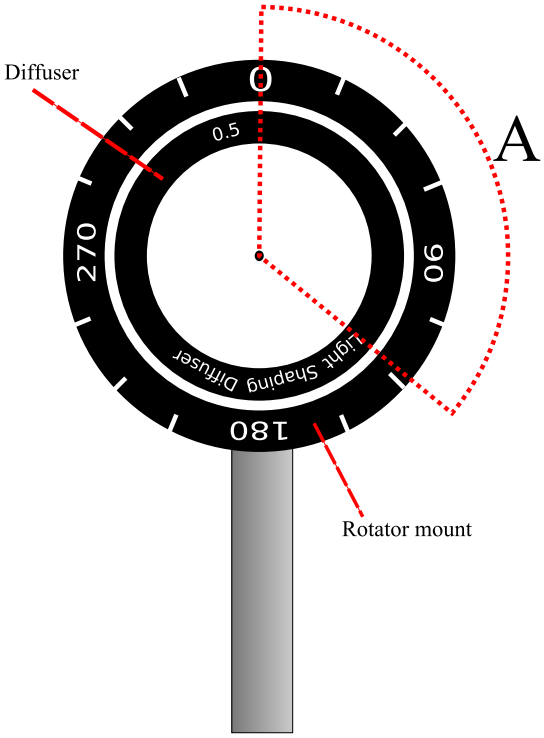

Figure 2: Orientation of the light shaping diffuser in the rotator mount. The angle A is the angle of the beginning of the letter L of the inscription LIGHT SHAPING DIFFUSER in the mount. For all diffusers the text is printed on the ring at the side of the rough surface of the plate. The angles A for the three diffusers are listed in Table 1.

4 Results classical speckle

4.1 Far field speckle statistics

For diffusers 1, 2 and 3 we measured 100 intensity profiles in the far field for each diffuser. Each picture has a different diffuser position. The two polarizers in the setup have parallel polarizations. In each picture the pump spot is on a different position on the diffuser. Summaries of the relevant far field speckle statistics can be found in Figure 3, Figure 4 and Figure 5. Each picture has the same composition of subfigures. The upper left subfigure shows a single speckle. On the upper right is the scaled intensity distribution of 100 speckles. The middle row shows a false color plot of the average intensity with a horizontal and vertical profile. The lower row shows a false color plot of the average autocorrelation with a horizontal and a vertical profile. The next sections will go deeper into the individual statistics. At the end of this chapter Table 2 presents all the relevant statistics per diffuser.

4.1.1 Average intensity

The average intensity over 100 intensity pictures for each diffuser is plotted in the middle rows of Figures 3, 4 and 5. These plots contain information about the opening angle of the diffusers. From Equation (6) we expect a Gaussian profile for the average intensity.

Diffuser 1 has an average intensity profile with a Gaussian shape. We fitted a Gaussian curve through the profile to obtain the fit parameters. The distribution is anisotropic with widths $\theta_x = 9.5$ mrad and $\theta_y = 7.5$ mrad, equivalent to $0.54°$ and $0.43°$. We note that this is of the same order as the specified $0.5°$ but that there are quite large variations.

The average intensity in the far field of diffuser 2 does not have a Gaussian distribution. The tails of the distribution are too strong. We can fit a Gaussian curve through the middle of the distribution with a width of $\theta_x = 7.1$ mrad by $\theta_y = 8.1$ mrad corresponding with $0.41°$ by $0.46°$. Using the full-width-half-maximum we obtain equal values.

The discrepancy between diffusers 1 and 2 is very surprising because the specifications of these diffusers are equal. The differences in average intensity are not explainable from randomness, the surfaces of the diffusers are really different.

The profiles of the average intensity of diffuser 3 is too rough to use it for a Gaussian fit. Due to the roughness also the full-width-half-maximum is inapplicable to give an accurate estimate of the width. We can make a Gaussian fit of the autocorrelation of the

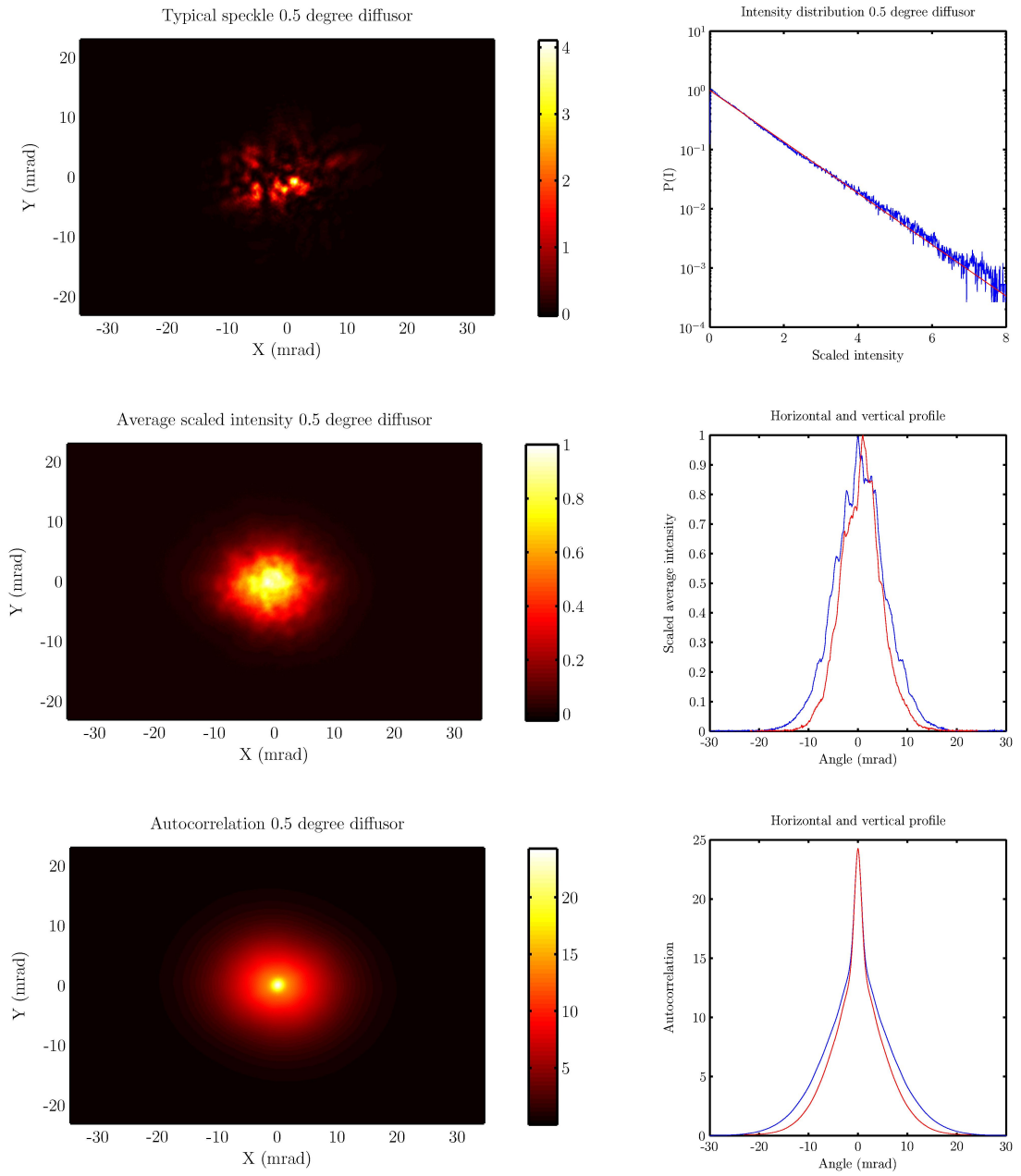

Figure 3: Characteristics obtained from 100 far field pictures of the diffuser 1. The upper left false color plot gives the scaled intensity distribution of a typical speckle. The upper right gives a histogram of occurrences of the scaled intensities for 100 speckle pictures. See Section 4.1.1 for details. The histogram is based on points for which the average intensity is at least half the maximum average intensity. The middle false color plot depicts the average intensity scaled to have maximum intensity 1. The right hand pictures are horizontal (blue) and vertical (red) profiles at the center of the distribution. The lower row gives the autocorrelation with a horizontal (blue) and vertical (red) profile.

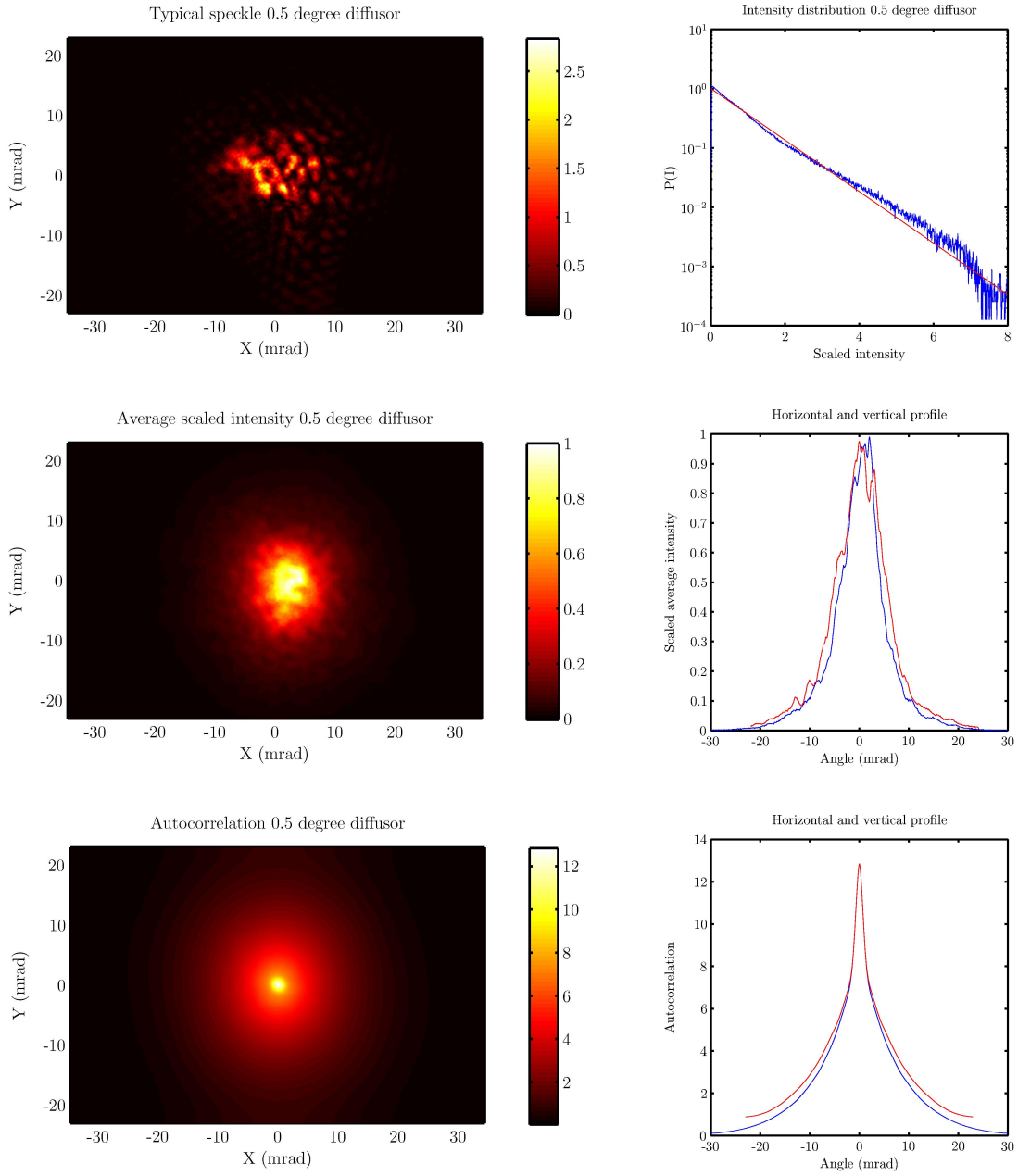

Figure 4: Characteristics obtained from 100 far field pictures of the diffuser 2. The upper left false color plot gives the scaled intensity distribution of a typical speckle. The upper right gives a histogram of occurrences of the scaled intensities for 100 speckle pictures. See Section 4.1.1 for details. The histogram is based on points for which the average intensity is at least half the maximum average intensity. The middle false color plot depicts the average intensity scaled to have maximum intensity 1. The right hand pictures are horizontal (blue) and vertical (red) profiles at the center of the distribution. The lower row gives the autocorrelation with a horizontal (blue) and vertical (red) profile.

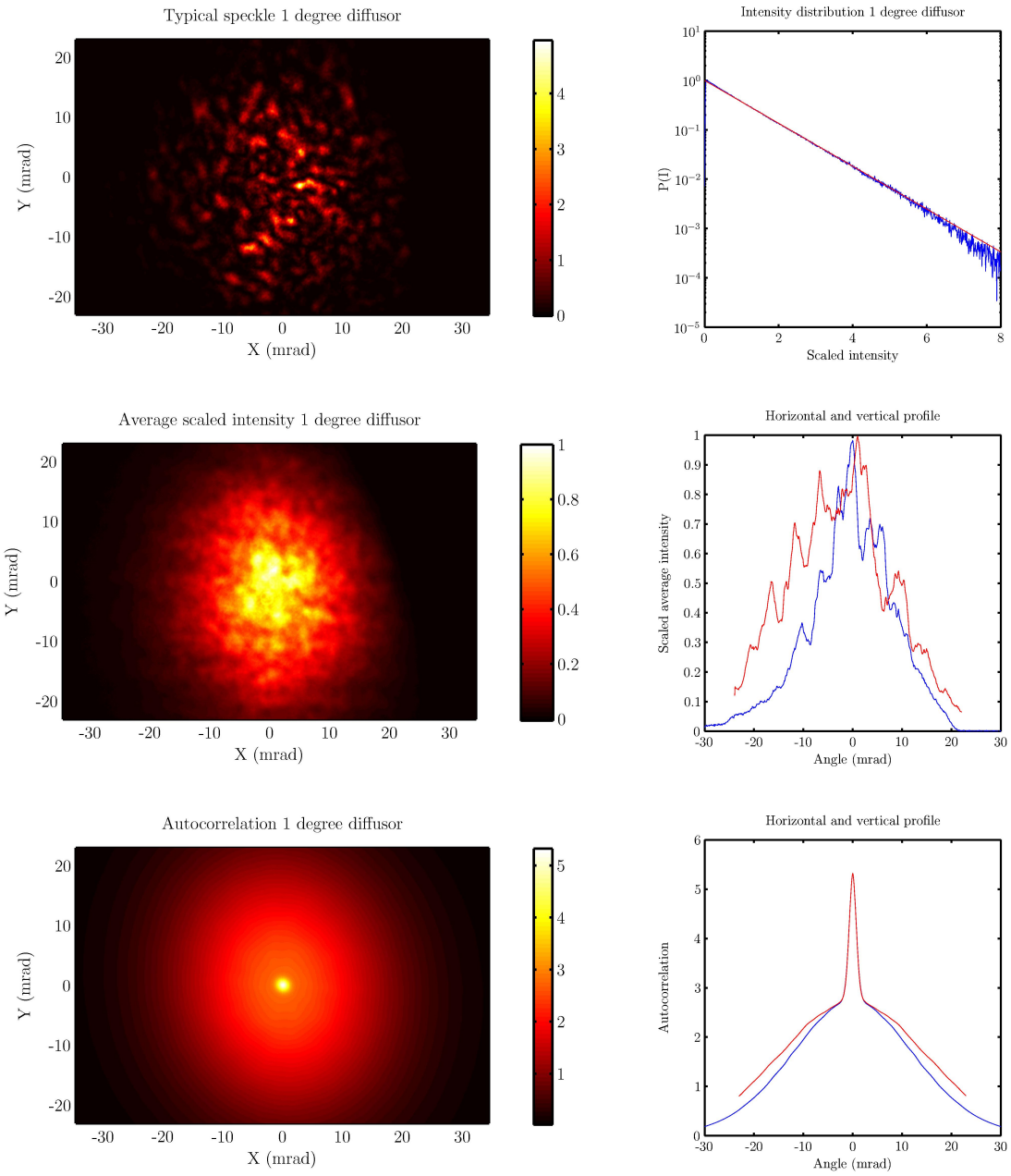

Figure 5: Characteristics obtained from 100 far field pictures of the diffuser 3. The upper left false color plot gives the scaled intensity distribution of a typical speckle. The upper right gives a histogram of occurrences of the scaled intensities for 100 speckle pictures. See Section 4.1.1 for details. The histogram is based on points for which the average intensity is at least half the maximum average intensity. The middle false color plot depicts the average intensity scaled to have maximum intensity 1. The right hand pictures are horizontal (blue) and vertical (red) profiles at the center of the distribution. The lower row gives the autocorrelation with a horizontal (blue) and vertical (red) profile.

average.[4] This function has a Gaussian profile and from it we can compute the opening angle of the diffuser. $\theta_x = 18.5$ mrad and $\theta_y = 21.3$ mrad, corresponding to 1.06° and 1.22°

4.1.2 Autocorrelation

The autocorrelation function with a horizontal and a vertical profile is given in the lower row of Figures 3, 4 and 5. From Equation (9) we expect the autocorrelation to have a double gaussian profile. The size of the shell is related to the opening angle of the diffuser, the size of the spike depends on the size of the laser spot.

Diffuser 3 is the only diffuser for which we measured a neat double Gaussian profile for its autocorrelation function.[5] A fit of this profile yields a width of the spike of $\theta_{\text{spike}} = 1.3$ mrad and two widths for the shell, $\theta_x = 18.5$ mrad and $\theta_y = 21.3$ mrad. Converting this to degrees we find diffuser 3 has two scattering axes with a width of 1.22° and 1.06°. The values correspond to the width obtained from the average intensity profile. The orientation of the long scattering axis with respect to the rotator mount is 5°. The size of the spike corresponds with a beam width of $w_0 = \lambda_0\sqrt{2}/\theta_{\pi\text{spike}} = 233$ μm. This is the expected value within the parameter uncertainty.

Also the autocorrelation plots of diffusers 1 and 2 have a spike width of $\theta_{\text{spike}} = 1.3$ mrad. Although the autocorrelation functions of diffusers 1 and 2 are not double Gaussian functions, so the concept of width is not applicable to these measurements, we do find that also these diffusers are anisotropic scatterers. This can be seen in the figures the autocorrelation function is an ellipsoid and the profiles are non overlapping. For diffuser 1 the effect is much stronger than for diffuser 2. The axis of anisotropy with respect to the mount can be measured for diffuser 1 is 88°. For diffuser 2 the measurement is less precise. Our best estimate is 15°.

We think it is likely that the difference between the expected autocorrelation function and the measured shape is a result of the pump spot size. In our derivation we assumed that the size of the pump spot was sufficiently large. The condition is that the far field opening angle (which is inversely proportional to the size of the pump spot) of the pump was much smaller than the opening angle of the diffuser. We think it is likely that for diffusers 1 and 2 this condition is not really met.

[4] Note that this is different from the average autocorrelation.

[5] In order to calculated the autocorrelation for diffuser 3 we had to add an extra dark area around the far field. The intensity profile of the speckles does not go to zero fast enough for diffuser 3. We enlarge the dark region to mitigate the otherwise unphysical correlation generated by the Fast Fourier Transform algorithm.

4.1.3 Intensity distributions

To make the intensity distributions we start with the individual speckle pictures and select all points where the average intensity is at least half the maximum average intensity. Then we compute the scaled intensity as the intensity in a speckle picture divided by the average intensity at that particular point over 100 speckle pictures with different diffuser positions . Along with the distribution from the data we plot the expected distribution from Equation (13). Please note that although the results are based on many observations the existence of speckles creates strong correlations between the individual points, thereby reducing the effective number of measurement points.

For diffuser 1 this yields a distribution based on $7 \cdot 10^5$ observations. The distribution of the diffuser is close to the expected distribution. However at the tail of the distribution we find small deviations. Please note that at the tails observations are scarce, we are not sure if these deviations are the result of the lack of observations or wether this is a fundamental effect.

For diffuser 2 this yields a diffuser of $8 \cdot 10^5$ observations. For this scatterer there is a mismatch between the expectation and the actual intensity distribution. We are not certain were this discrepancy originates, but it will probably have to do with the heavy tails in the average intensity of diffusor 2.

For diffuser 3 this yields a diffuser of $3 \cdot 10^6$ observations. For this diffuser we note that the distribution is close to the expectation.

The exponential distribution for the intensities is expected when the far field of the electric field vector $\boldsymbol{E}$ is the result of many random contributions. According to the central limit theorem the distribution of $\boldsymbol{E}$ is Gaussian and in appendix A we derived that the distribution for the intensity I should be exponential.

4.1.4 Contrast

For each speckle picture we computed the contrast C. The contrast is a measure of the visibility of the speckle. Inside each speckle picture we isolated an area, much larger than a single speckle, but small enough not to let the shell function of the speckle come into play, using the same criterium that we used for the intensity distributions. The area under consideration is comparable to the area we will use for in our biphoton measurements. Using this area we computed the contrast C of each speckle using Equation (16). For diffuser 1 we find an average contrast for the speckles of 0.90. The maximum contrast 1.36 and the minimum is 0.66. Diffuser 2 has an average contrast of 0.93 with a maximum of 1.30 and a minimum of 0.60. Diffuser 3 has an average contrast of 0.89 with a maximum

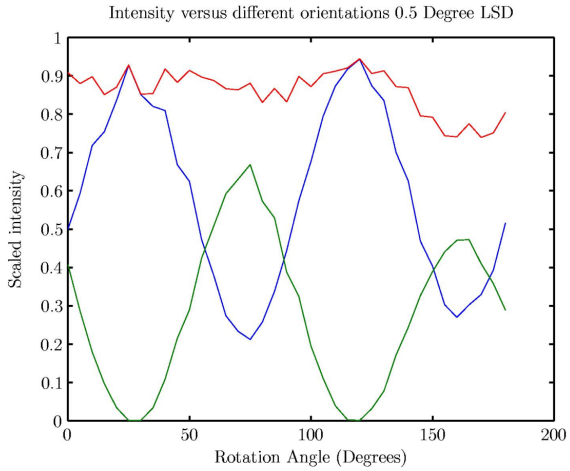

Figure 6: The transmission of diffuser 1 for two geometries versus the diffuser orientation. The blue line is the transmission in the parallel polarization, the green line in the crossed polarization and the red line is the total. The transmission is computed as the power (summed intensity) scaled with the power in absence of a second polarizer.

of 1.22 and a minimum of 0.66. The contrast distributions are equal for all diffusers. Deviations are likely to be the result of the limited number of speckles in the contrast region. We conclude that there are large variations in the visibility of speckle patterns due to the statistical nature of the speckle.

4.2 Birefringence of diffuser plates

The incoming light on the diffuser is vertically polarized. Directly behind the diffuser we placed a second polarizer. When this second polarizer also has the vertical polarization we will speak of parallel polarizations and if the second polarizer has a horizontal polarization we will refer to this as cross polarized. The diffuser is placed in a rotator mount. We measured the total intensity in the near field for various orientations of the diffuser and constructed a graph for both parallel and crossed polarizations. The results are presented in Figure 6. We find that diffuser 1 shows a very strong birefringence, for certain orientations more than half of the incoming light is transferred to the other polarization channel. We conclude this because the transmission for the different geometries shows a periodic behaviour with a period of 90°. This corresponds to birefringence as both alignment of the fast axis and the incoming polarization direction and alignment of the slow axis and

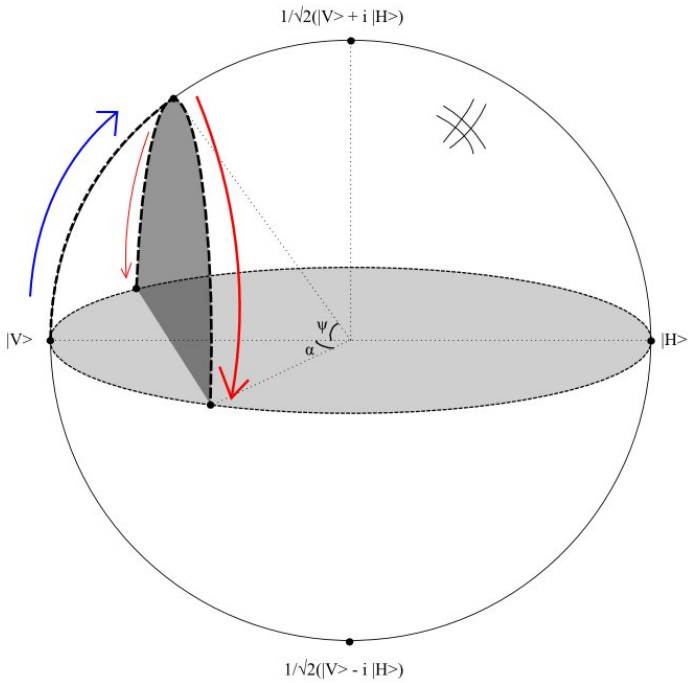

Figure 7: The Poincaré sphere with the various polarization states, $|H\rangle$ for horizontal polarization, $|V\rangle$ for vertical. The effect of the diffuser is indicated by the blue arrow. The effect of the quarter wave plate is indicated by the red arrows. ψ and α indicate the angles made by the blue and the red arrows respectively. 1.

the incoming polarization direction yield a zero contribution to the crossed polarization channel. Note that the percentage of transmission in the parallel and crossed polarization are not completely equal if we rotate the diffuser 90°. This is probably because the position on the diffuser is not fixed when changing the orientation, and the transfer will probably depend on the position of the pump spot.

We checked whether the orientation of the slow and fast axis of the diffuser is constant or also position dependent. We placed the diffuser in a large spot with incoming polarized light and looked at the cross polarized transmission. Because it was possible to totally darken the image when changing the orientation of the diffuser we conclude that the orientation of the fast and the slow axis must be equal all over the diffuser.

We placed a quarter wave plate behind the diffuser, followed by a polarizer. First we maximized the light in the crossed polarization by rotating the diffuser. We then minimized to outgoing light by changing the orientation of the quarter wave plate and the second polarizer. This procedure is indicated on the Poincaré sphere in Figure 7. The surface of this sphere presents all possible polarization states: on the equator are the linearly polarized states, and on the poles the perfect circular states. The diffuser moves the state along the blue line. The quarter wave plate then moves the state along one of the red lines. The plate rotated over 90 degrees moves it along the other red line. After passing through the blue and the red line the state is a point on the equator again and the light can be fully blocked using a polarizer. The difference in orientations of the polarizers for the two points on the equator is related to the angle ψ.

$$\psi = 180^\circ - (\alpha_1 - \alpha_2). \tag{17}$$

From our measurements it follows that $\psi = 106^\circ$ for diffuser 1. This angle indicates that the birefringence in the diffuser is just a little bit more than that of a quarter wave plate. From the transmission in the minimum we can obtain a measure for the variation in ψ

$$T_m = \frac{1}{2}\left[1 - \cos(2\Delta\psi)\right], \tag{18}$$

where the minimum transmission is 0.02 for diffuser 1. From this we can compute that the variation $\Delta\psi = 0.14$ rad $= 8^\circ$. This illustrates why the transmission in Figure 6 varied for the two different spots on the diffuser.

For diffuser 3 we also did this measurement. We found that $\psi = 20^\circ$ and $\Delta\psi$ is negligible. We conclude that for diffuser 3 the birefringence plays a less important role than in diffuser 1.

	Opening angle			Birefringence		
	Long	Short	Orientation	Angle	Variation	Orientation
Diffuser 1	$0.54°$	$0.43°$	$88°$	$106°$	$8°$	$153°$
Diffuser 2	$0.46°$	$0.41°$	$15°$	-	-	-
Diffuser 3	$1.21°$	$1.06°$	$5°$	$20°$	$0°$	$95°$

Table 2: Summary of the properties of the various diffuser plates we used. The long and short opening angle refer to the best estimations we can make of the opening angle based on far field statistics. The orientations refers to the angle that the long scattering axis makes in the rotator mount. In the birefringence columns the angle specifies how birefringent the sample is, where $180°$ is a half-lambda-plate. The second column gives the variation in this angle at different positions on the diffuser and the last column gives the orientation of the fast axis in the rotator mount.

5 Theory biphoton speckle

In this section we will outline the theory of biphoton speckle. The notation will be close to that of the classical speckle. When we generate photon pairs using SPDC, one photon holds information about the other photon. The information about entanglement is contained in the field [**?**]

$$A(\boldsymbol{x}_1, \boldsymbol{x}_2) = \left\langle 0|\widehat{E}^{(+)}(\boldsymbol{x}_1)\widehat{E}^{(+)}(\boldsymbol{x}_2)|\Psi\right\rangle \tag{19}$$

The field A is the expectation of the product of two electric fields operators at detector positions $\boldsymbol{x}_1$ and $\boldsymbol{x}_2$ for the transition of a paired photon state Ψ to vacuum state 0. The electric field operators are proportional to the creation and annihilation operators

$$\widehat{E}^{(+)} \sim \widehat{a} \tag{20}$$
$$\widehat{E}^{(-)} \sim \widehat{a}^{\dagger}. \tag{21}$$

Although the origin of the biphoton field A is purely quantum mechanical, in calculations we can treat it as a classical quantity.[6] The dimension of A is the dimension of a squared electric field. Instead of directly measuring A we measure the coincidence counts R_{cc}. A coincidence occurs when two photons enter two different detectors within the same time frame. These coincidences are proportional $|A|^2$. The relation between the two photon field A and the coincidence counts R_{cc} are comparable to the relation between the intensity I and the electric field $\boldsymbol{E}$ in the single photon case.

The biphoton field of the SPDC beam at the crystal center is [**?**]

$$A_{\text{SPDC}}(\boldsymbol{x}_1, \boldsymbol{x}_2) = A_0 E_p \left(\frac{\boldsymbol{x}_1 + \boldsymbol{x}_2}{2}\right) \int \text{sinc}\left[\frac{\lambda_p L}{8\pi n_0}\boldsymbol{q}_-^2\right] \exp\left[\frac{1}{2} i\,(\boldsymbol{x}_1 - \boldsymbol{x}_2)\cdot\boldsymbol{q}_-\right] d\boldsymbol{q}_-. \tag{22}$$

where $\boldsymbol{x}_1$ and $\boldsymbol{x}_2$ are the transverse position vectors for the two photons and the integration element $\boldsymbol{q}_-$ represents the difference in the far field wave vectors. The parameters that define the field are the size of the crystal L, the frequency of the pump λ_p and the refractive index in the crystal for the low energy wavelength n_0. We can simplify this expression if we approximate the sinc function with a Gaussian [**?**]

$$\text{sinc}[b\,\boldsymbol{q}_-^2] \approx \exp[-ab\,\boldsymbol{q}_-^2], \tag{23}$$

[6] We may do so because the propagators of the biphoton field are equal to the propagators of classical electrical fields.

with $a = 0.455$. Using this approximation and filling in the field of the pump E_p we can compute

$$A_{\text{SPDC}}(\boldsymbol{x}_1, \boldsymbol{x}_2) = A_0 \exp\left(-\frac{(\boldsymbol{x}_1 + \boldsymbol{x}_2)^2}{4w_p^2} - \frac{(\boldsymbol{x}_1 - \boldsymbol{x}_2)^2}{w_-^2}\right). \tag{24}$$

Here w_p is the size of the pump spot and

$$w_- = \sqrt{\frac{2a\lambda_p L}{\pi n_0}} \tag{25}$$

is called the phase matching parameter, which can be interpreted as the distance between the two photons of a photon pair.

Now we will introduce the dimensionality of the spatial entanglement. This dimensionality is captured by the number of spatial modes and related to the coherence of the beam on a single photon level. The incoherence will decrease the contrast of speckles in the far field intensity. The intensity can be computed from the field A using

$$I(\boldsymbol{x}) \sim \int A(\boldsymbol{x}, \boldsymbol{x}')^* A(\boldsymbol{x}, \boldsymbol{x}') d\boldsymbol{x}'. \tag{26}$$

We define the number of modes

$$N_m \equiv \frac{\int \widehat{I}_p(\boldsymbol{x}') d\boldsymbol{x}' \int \widehat{I}_{\text{FF}}(\boldsymbol{\theta}') d\boldsymbol{\theta}'}{\lambda_p^2}, \tag{27}$$

as the optical etendue of the setup where I_p is the intensity in the crystal and I_{FF} is the intensity in the far field of the crystal. The hat operator $\widehat{\cdot}$ scales the intensity function with the peak intensity. For the SPDC beam the number of modes is

$$N_m = \left(\frac{w_p}{w_-}\right)^2. \tag{28}$$

It is a measure of the spatial coherence on the single photon level.

The diffuser is placed in the near field image of the crystal. Directly behind the diffuser the field A picks up a random phase based on the random functions $\phi(\boldsymbol{x_1})$ and $\phi(\boldsymbol{x_2})$ for both photons

$$A_d(\boldsymbol{x}_1, \boldsymbol{x}_2) = A_{\text{SPDC}}(\boldsymbol{x}_1, \boldsymbol{x}_2) \exp\left(i\boldsymbol{\phi}(\boldsymbol{x}_1) + i\boldsymbol{\phi}(\boldsymbol{x}_2)\right). \tag{29}$$

Using a Fourier transform we can propagate this near field A_d to the far field and find its dependence on the angles $\boldsymbol{\theta}_1$ and $\boldsymbol{\theta}_2$ in the far field [**?**]. Because the dependence on two detector positions we have to integrate twice,

$$A_{\text{FF}}(\boldsymbol{\theta}_1, \boldsymbol{\theta}_2) = \int\int A_d(\boldsymbol{x}'_1, \boldsymbol{x}'_2) \exp\left(\frac{-2\pi(\boldsymbol{\theta}_1 \cdot \boldsymbol{x}'_1 + \boldsymbol{\theta}_2 \cdot \boldsymbol{x}'_2)}{\lambda_0}\right) d\boldsymbol{x}'_1 d\boldsymbol{x}'_2. \tag{30}$$

We can now compute the speckle statistics in the far field. Using the analogy with the classical speckle we find that the second moment in coincidences[7] can be rewritten as a function of the first order statistics of the coincidences plus the second order statistics of the A field.[8] Using Gaussian statistics, we find that $\Gamma^{(4)}$ in the far field of the diffuser is

$$\begin{aligned} \Gamma^{(4)}(\boldsymbol{\theta}_1, \boldsymbol{\theta}_2, \boldsymbol{\theta}'_1, \boldsymbol{\theta}'_2) &= \langle R_{cc}(\boldsymbol{\theta}_1, \boldsymbol{\theta}_2) R_{cc}(\boldsymbol{\theta}'_1, \boldsymbol{\theta})'_2 \rangle_D \qquad (31) \\ &= \langle R_{cc}(\boldsymbol{\theta}_1, \boldsymbol{\theta}_2) \rangle_D \langle R_{cc}(\boldsymbol{\theta}'_1, \boldsymbol{\theta}'_2) \rangle_D + \left| \langle A^*(\boldsymbol{\theta}_1, \boldsymbol{\theta}_2) A(\boldsymbol{\theta}'_1, \boldsymbol{\theta}'_2) \rangle_D \right|^2. \end{aligned}$$

Here $\boldsymbol{\theta}_1$ and $\boldsymbol{\theta}_2$ are two-dimensional vectors with the angular position of detectors 1 and 2. The primed coordinates are also two-dimensional vectors for the positions of another pair of detectors 1 and 2. It will be useful to introduce new coordinates that represent the difference in position of the detector modes and their sum

$$\boldsymbol{\theta}_s \equiv \boldsymbol{\theta}_1 + \boldsymbol{\theta}_2 \tag{32}$$

$$\boldsymbol{\theta}_d \equiv \boldsymbol{\theta}_1 - \boldsymbol{\theta}_2 \tag{33}$$

Using these coordinates we can express the autocorrelation $\Gamma^{(4)}$ in terms of four functions based on these sum and difference coordinates

$$\Gamma^{(4)}(\boldsymbol{\theta}_1, \boldsymbol{\theta}_2, \Delta\boldsymbol{\theta}_1, \Delta\boldsymbol{\theta}_2) = |f_{\text{shell}}(\boldsymbol{\theta}_s) g_{\text{shell}}(\boldsymbol{\theta}_d)|^2 \times \left[1 + |f_{\text{spike}}(\Delta\boldsymbol{\theta}_s) g_{\text{spike}}(\Delta\boldsymbol{\theta}_d)|^2\right] \tag{34}$$

The angles with a delta indicate the difference of a certain coordinate with its primed counterpart. The sharpest angular dependence is present in the function

$$f_{\text{spike}}(\Delta\boldsymbol{\theta}_s) = \exp\left(-\left(\frac{\pi w_p \Delta\boldsymbol{\theta}_s}{\lambda_0}\right)^2\right). \tag{35}$$

This function has the same width as the spike function present in the classic photon speckle autocorrelation. This implies that the biphoton speckles and the single photon

[7] We will write $\Gamma^{(4)}$ with a superscript 4 because it is the fourth moment in electrical fields.

[8] We use the complex Gaussian moment theorem [**?**]. This theorem is used to compute the second moment in intensities $\Gamma^{(2)}$ in Section B of the appendix.

speckles have the same size if we scan for speckles using one detector while keeping the other detector fixed.

The second function in the spike is the function

$$g_{\text{spike}}(\Delta\boldsymbol{\theta}_d) = \exp\left(-\left(\frac{\pi w_- \Delta\boldsymbol{\theta}_d}{2\lambda_0}\right)^2\right). \tag{36}$$

It depends on the opening angle of the SPDC input. This function determines the size of the structures when we scan in difference coordinates. It also determines over what angles the biphoton speckle observed with detector 1 is displaced when detector 2 is displaced and for what angle the speckle pattern in detector 1 starts changing.

The shell functions depend on the opening angle of the diffuser. These functions will not have much influence on our measurement because we generally detect a very small angle compared to the opening angle of the diffuser.

6 Setup biphoton speckle

An overview of the setup for the biphoton experiment is given in Figure 8

Using a Krypton ion gas laser (Coherent Innova 300) we generate a pump beam with $\lambda_p = 413.1$ nm. The power of the laser varies from experiment to experiment but is generally between 170 mW and 240 mW. We indicated the beam consisting predominantly of the high energy blue photons with a blue line. After the blue photons are filtered out we indicated the light consisting of red photon pairs with a red line.

We focus the pump beam on a 5 mm long periodically poled $KTiOPO_4$ crystal (PPKTP) with lens A ($f = 1000$ mm). The size of the pump spot is $w_p = 170$ μm. The nonlinear optical process of spontaneous-parametric-downconversion (SPDC) converts some of the blue pump photons into pairs of red photons. The wavelength of the outgoing photons is $\lambda_0 = 826$ nm. However the beam exiting the crystal is still dominated by the blue photons. We place a GaP plate to filter out the blue photons. Now the beam is dominated by pairs of infrared photons, indicated by a red line. The A field that describes the structure of this beam is given by Equation (19) where the parameter $w_- = 18$ μm (see Equation (25)). We will refer to this as the SPDC beam.

We focus the SPDC beam onto the random phase plate using a telescope system. This $f - 2f - f$ system uses lenses B and C, both with $f = 200$ mm, to make an exact one-to-one image of the near field of the crystal on the diffuser plate. Both lenses are placed using the autocollimation method (see Section D). The incident A field on the diffuser (Near Field 2) is equal to the near field at the crystal (Near Field 1). The diffuser plate we will use is diffuser 3, with an opening angle of approximately 1°. The openings angle is large enough in relation to the area we will scan so that we do not have to take the shell function from Equation (9) into consideration. Choosing a diffuser with a larger openings angle will only reduce the reduce our intensity in the far field, complicating our measurement. The diffuser is placed in a rotator mount and the orientation is chosen so that the fast axis of the plate is parallel to the vertical axis, which is also the polarization axis of the SPDC beam. The rough surface of the diffuser is placed toward the incident SPDC beam.

Behind the diffuser, we use a $f = 300$ mm (and later a $f = 250$ mm) lens in an $f - f$ system to make an image of the far field of the diffuser (Far Field 2). The system is aligned using the autocollimation method. Within the $f - f$ system, behind lens C, we place a beam splitter with a 50-50 distribution, to split the photon pair in two outgoing directions. Please note that because of the beam splitter we lose half our coincidence counts because there is only a 50% probability that the photons of a pair choose two different paths through the beam splitter. Both photons of a pair have to enter another

detector to be counted as a coincidence.

The far field image (Far Field 2) is monitored with two scannable detectors. Each detector mode comprises of an object lens and a single mode fiber. The object lens (Geltech $f = 8$ mm) is used to focus the incoming light into the fiber (with a mode field diameter of MFD $= 5.6$ μm) Both detectors are mounted on two stages which can be precisely moved in both transverse directions using actuators. In front of the object lenses of the detector modes we placed two filters that transmit a range of only 5 nm at a bandwidth of 826 nm.

We verified that we had a focus on the fiber by coupling a laser to the other side of the fiber and shooting back laser light through the detection mode. We tweaked each stage in the z-direction so that the laser beam was focussed at the point where the far field of the diffuser was projected. We used a chopper for this alignment procedure.

The size of the detector modes depends on the focal distance of lens D. For $f = 300$ mm the size of the detector mode in Far Field 2 is $\theta_D = 0.25$ mrad. For $f = 250$ mm we measured $\theta_D = 0.40$ mrad. Based on a pump size of $w_p = 170$ μm we expect speckles with a size of $\theta_p = 1.5$ mrad. The resolution for both systems is high enough to observe speckles. We expect the system with the 250 mm lens to have more counts and yield a better signal-to-noise ratio.

Both fibers are connected to single photon counters (SPCM-AQR). The generated electric pulses are routed to a fast AND gate that serves as a coincidence circuit with a specified gate time of $\tau_{\text{gate}} = 1.73$ ns. The coincidences counts are integrated over $\tau_{\text{int}} = 4$ s for each position of the detectors to obtain the average coincidence count rate.

Accidental counts are not a manifestation of the biphoton field but just two uncorrelated photons that happen to enter the detector at the same time. The accidental count rate is estimated by

$$R_{\text{acc}} = R_{s,1} R_{s,2} \tau_{\text{gate}} \tag{37}$$

where $R_{s,1}$ and $R_{s,2}$ are the single photon count in detector 1 and detector 2. The raw coincidences are corrected with these accidentals to obtain the adjusted coincidence counts. Correcting is important because the accidental count rate is about the same order as the corrected coincidences.

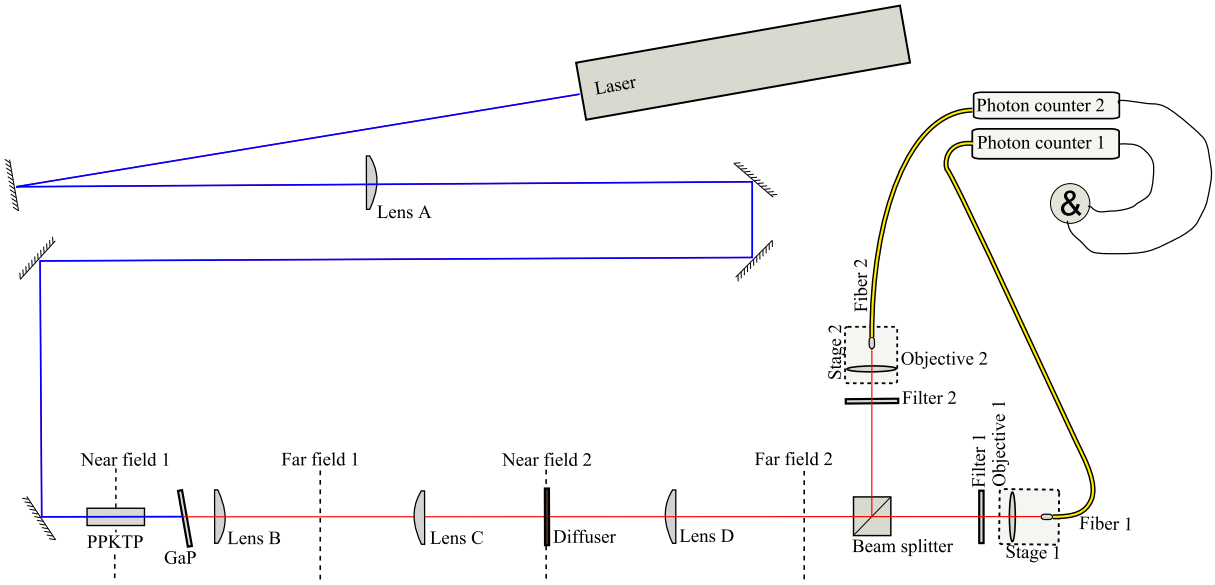

Figure 8: Schematic picture of the experimental setup for the biphoton speckle experiment. A beam from the laser is focussed onto a PPKTP crystal (Near Field 1) using lens A. Directly behind the crystal the remaining blue light is filtered out using a AR-coated wafer of GaP. A one-on-one near field (Near Field 2) image of the crystal is made onto a diffuser plate using lenses B and C. Behind the diffuser lens D makes a far field image (Far Field 2) of the diffuser plate on the detector modes. Both detector modes are separated by a beam splitter. The detector modes are composed of a fiber and an object lens that focusses the light on the fiber. Both detectors are indicated by the dotted areas denoted as Stage 1 and Stage 2. The fibers are connected to photon counters 1 and 2. The beam with predominately blue light is given in blue and the beam which is predominately composed of infrared photon pairs is colored red.

7 Results biphoton speckle

Using the setup given in Figure 8 we generated biphoton speckle. The biphoton speckle is a function of the positions of two detectors $\boldsymbol{x}_1$ and $\boldsymbol{x}_2$. In this section we will show biphoton speckle where at a single photon level speckle is absent. Both detectors have a x and y position which implies biphoton speckle depends on 4 coordinates. We will consider three approaches to show the properties of the speckle. In the next section we will discuss a fixed detector scan where one detector is kept fixed and the other detector makes a scan in the x and y direction. The other sections describe approaches where the detectors are moving parallel (and the difference in detector position is kept constant) and where the detectors are moving antiparallel (where the average position of the detectors is kept constant). In the last section we discuss preliminary results on the dimensionality of entanglement of our SPDC beam. We truncated the light with an aperture to allow fewer spatial modes and found that not only the biphoton structure changes and but also single photon speckle reappears. At the end of the chapter the parameters of the biphoton field estimated from the various speckle experiment are summarized in table 3.

7.1 Single fixed, single moving detector scan

For our first biphoton speckle picture we fixed the position of detector 2 and made a scan in the x and y direction using detector 1. The results are depicted in Figure 9. Please note that the depicted coincidence counts corrected for the accidental counts calculated from Equation (37). Typical values for the accidental rates are $250\ c/s$ for Figure 9 and $600\ c/s$ for Figures 10 to 12. The raw counts are a Poisson process and cannot be negative. Due to statistical variations the adjusted counts can have negative values.

The SPDC light is very incoherent as there are $N_m \approx 90$ modes (Equation (27)). This results in a low visibility of speckles in the single photon counts. The measured contrast from Equation (16) is $C = 0.08$. The coincidence counts however show fully developed speckle pattern with a measured contrast of $C = 1.1$. From the width of the spike in the autocorrelation function we find that the average speckle has a width of $\theta_{\text{spike}} = 1.0$ mrad. Equation (35) relates the size of the speckle to the pump size. The implied pump size is $w_p = \lambda_0/\pi 1.0\ \text{mrad} = 263\ \mu\text{m}$. We attribute the difference between this value and the actual pump size $w_p = 170\ \mu$m to the variations in speckle size. This is confirmed by Table 3 which shows big variations in parameters implied from the speckle size.

Figure 10 shows an additional scan of detector 1, keeping detector 2 fixed on the upper left. On the upper right is a scan at the same position of the diffuser when scanning detector 2 keeping detector 1 fixed. Both speckle pattern look very much alike. The

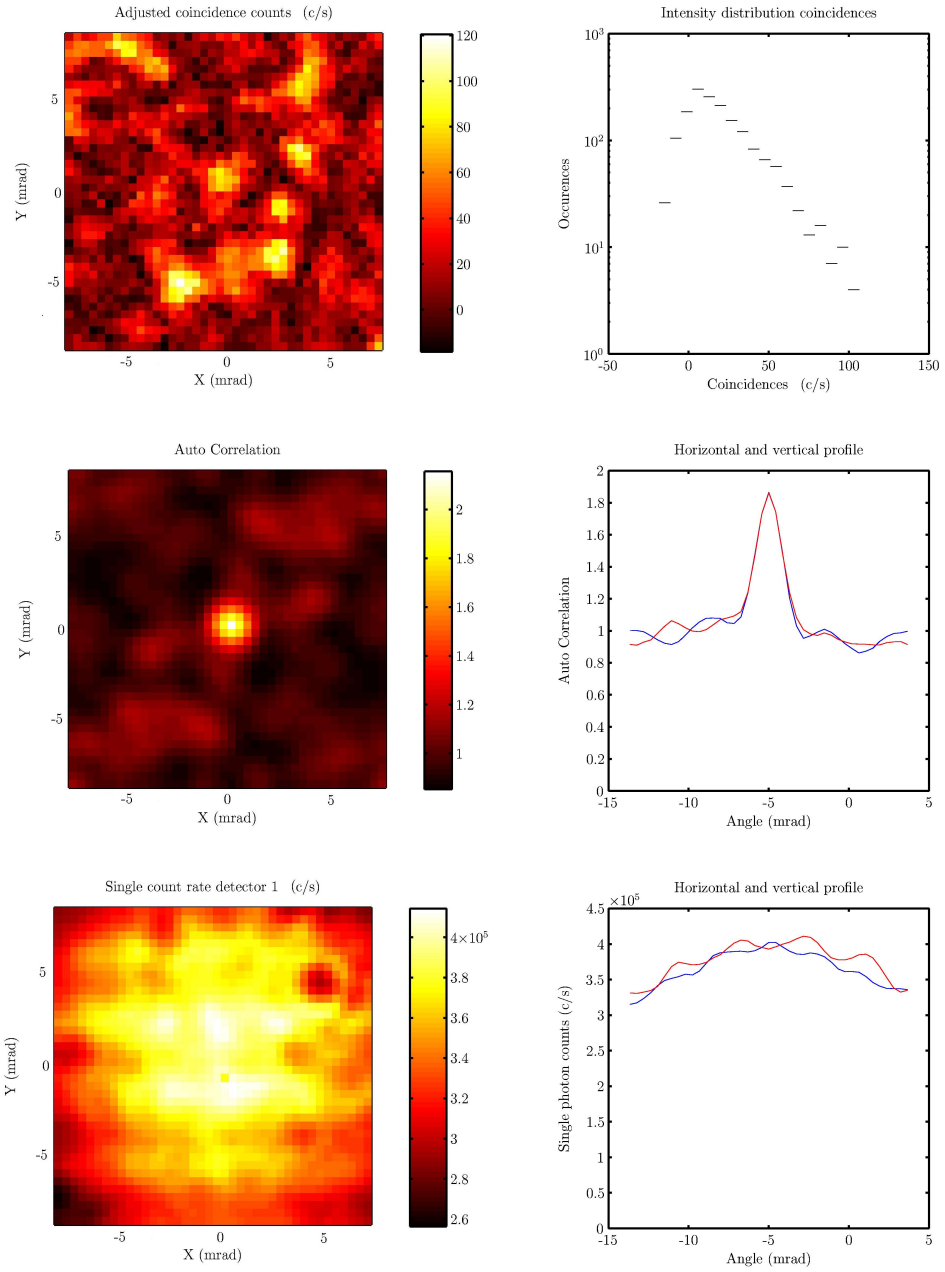

Figure 9: The coincidence counts for a 1° diffuser plate in a SPDC beam. The upper left figure depicts the coincidence counts for different angles of detector 1. The upper right is an histogram of these coincidence counts The middle row shows the autocorrelation with on the right hand side a horizontal (blue) and vertical (red) profile. The lower row gives the single photon counts in detector 1, with a horizontal (blue) and a vertical (red) profile.

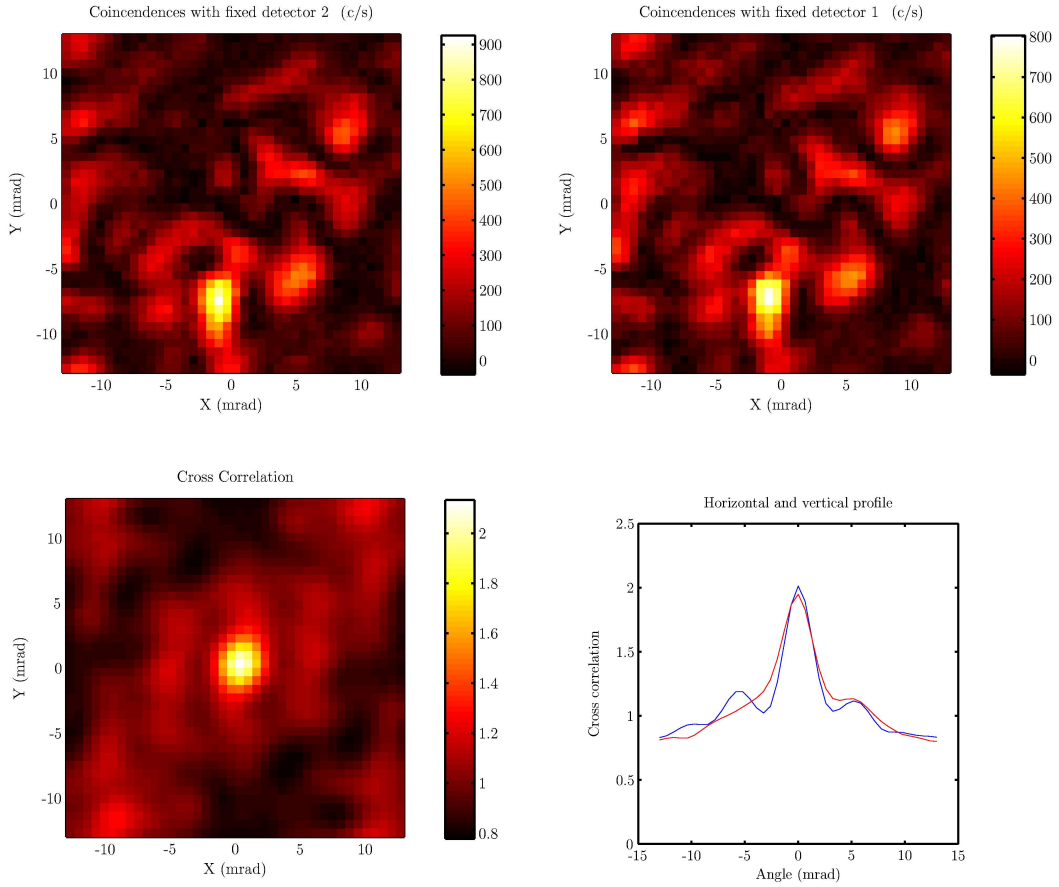

Figure 10: Coincidence counts for a scan with detector 1, keeping detector 2 fixed (upper left) and a scan with detector 2 keeping detector 1 fixed (upper right). The lower row gives their cross correlation, with a horizontal (blue) and a vertical (red) profile.

speckle size in both pictures is 2.1 mrad corresponding to an implied pump size from both pictures of $w_p = 125$ μm. The correlation between these pictures, defined as

$$\rho \equiv \frac{\langle R_{cc,1} R_{cc,2} \rangle_{XY}}{\sqrt{\langle R_{cc,1}^2 \rangle_{XY}} \sqrt{\langle R_{cc,2}^2 \rangle_{XY}}}, \tag{38}$$

is 0.95. As expected there is no difference between the detectors and therefore they should show an identical speckle picture. The resolution of the pictures given in Figure10 differs from the initial biphoton speckle measurement in Figure9 as the 300 mm lens in the far field imaging system is replaced with a 250 mm lens. This results in a great increase in the signal-to-noise ratio.[9]

We find that if we move the one detector over a small angle (order of 1 mrad) the biphoton speckle pattern recorded when scanning the other detector is displaced over the same distance but shows approximately the same structure. If we move over larger angle (10 mrad) we find that the speckle pattern will also change.[10]

7.2 Parallel moving detectors

The summed coordinate and difference coordinate of the two detectors are defined as $\boldsymbol{\theta}_s = \boldsymbol{\theta}_1 + \boldsymbol{\theta}_2$ and $\boldsymbol{\theta}_d = \boldsymbol{\theta}_1 - \boldsymbol{\theta}_2$. A scan in the summed coordinate means that the difference coordinate $\boldsymbol{\theta}_d$ is kept constant and $\boldsymbol{\theta}_s$ is moved. The physical interpretation is that both scanners move parallel in the far field.

Figure 11 still shows an illustration of the effects of a summed coordinate scan. The upper picture gives a fixed detector scan, which means $\boldsymbol{\theta}_1$ varies and $\boldsymbol{\theta}_2$ is constant. As a result both $\boldsymbol{\theta}_s$ and $\boldsymbol{\theta}_d$ are variable. The middle picture gives a summed coordinate scan where there is only a change in $\boldsymbol{\theta}_s$. The axis denote the displacement by single detectors $\boldsymbol{\theta}_1 = \boldsymbol{\theta}_2$, not the summed coordinate. In comparison to the fixed detector biphoton speckle it is possible to see smaller structures keeping the same displacements but displacing both scanners. The speckle width in the original is 1.7 mrad. The summed coordinate version has a speckle width of 1.0 mrad. Theoretically, we expect a factor 2 between the original speckle width and the width in the summed coordinate speckle. However only a single speckle picture has been measured. We believe that the width of the spike in the autocorrelation can be very dependent on the presence of several large speckles. Because the summed coordinate scan has more small speckles in the outer edges the

[9] For an explanation of this result please refer to Section 6.

[10] These results are not included.

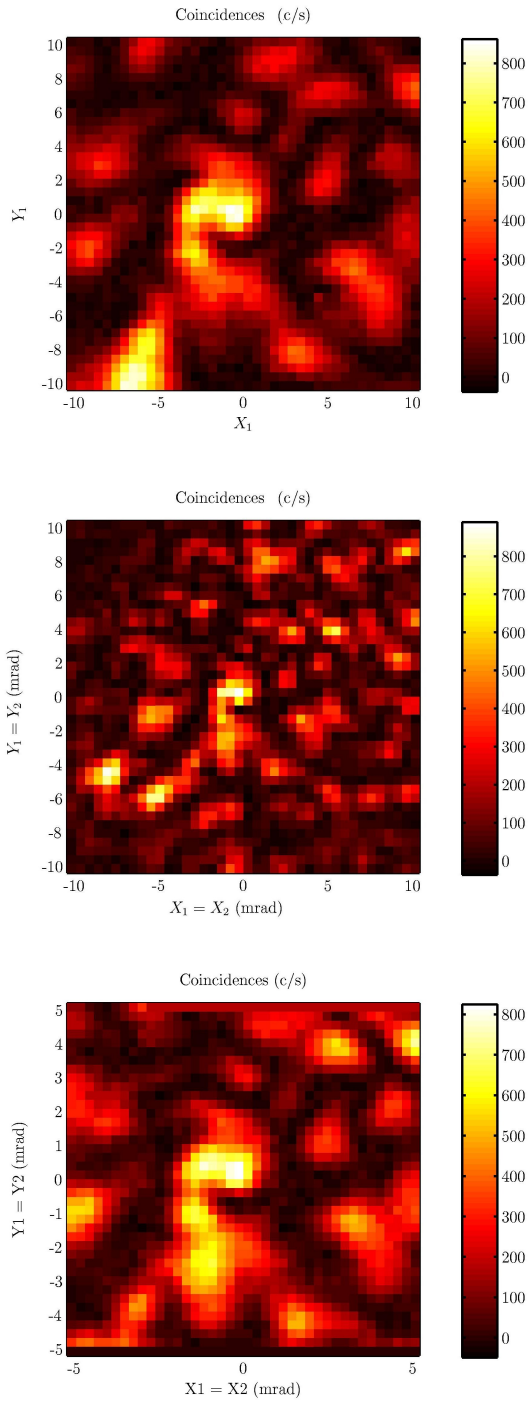

Figure 11: The upper image is a biphoton speckle picture using the position of detector 1 keeping detector 2 constant. The middle image is a biphoton speckle using summed coordinates. Both detectors 1 and 2 are moved keeping their difference coordinate constant. The scale in the second picture denotes the displacement of a single detector. The lower picture is a summed coordinate scan at double resolution. The correlation defined by Equation (38) between the upper biphoton speckle and this zoomed version is 0.78.

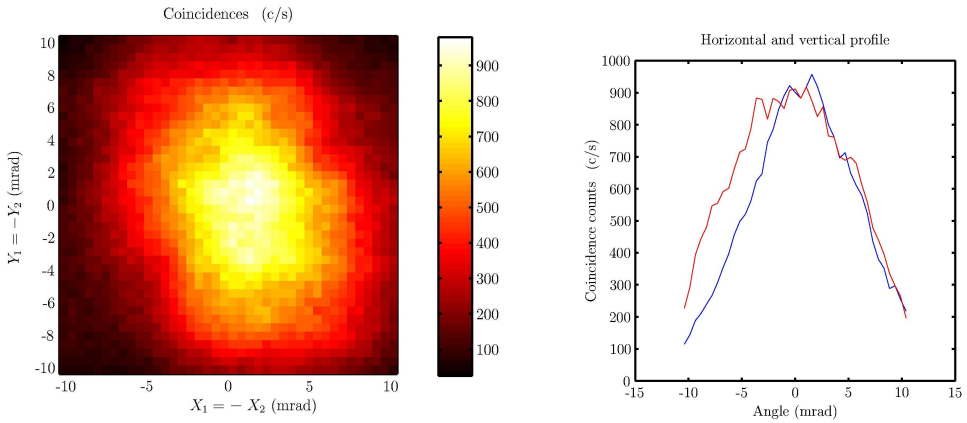

Figure 12: Coincidence counts in a difference coordinates scan, with a horizontal (blue) and a vertical (red) profile.

difference in width is larger than the expected factor. Our believe is confirmed by the observation that the zoomed version of the middle picture of Figure 11, namely the bottom picture, has a width of $1.7/2 = 0.85$ mrad. This zoomed picture shows that there is a strong resemblance between the original speckle and the zoomed speckle in summed coordinates. The correlation coefficient between both pictures is $\rho = 0.78$. The strong correlation between the summed coordinate scan and the zoomed fixed detector scan is a great support for the theoretic results that the function f_{spike} given in Equation (35) defines the smallest structures visible in the biphoton speckle.

Based on the fixed detector scan in the top of Figure 11 the expectations for the parameter $w_p = \lambda_0/\pi 1.7$ mrad $= 154$ μm. The summed coordinated scan in the middle of Figure 11 gave an implied parameter of $w_p = \lambda_0/2\pi 1.0$ mrad $= 131$ μm. The zoomed version of the summed coordinate scan on the bottom of Figure 11 again yielded $w_p = \lambda_0/\pi 1.7$ mrad $= 154$ μm The measured value is $w_p = 170$ μm. We think these values implied by the speckles correspond to the measured pump width within the uncertainty generated by the random speckle patterns.

7.3 Anti-parallel moving detectors

In this section we will investigate a scan with anti-parallel moving detectors. Detector 2 is programmed to scan exactly in the opposite direction of detector 1. Mathematically we keep $\boldsymbol{\theta}_s = \boldsymbol{\theta}_1 + \boldsymbol{\theta}_2$ constant and vary $\boldsymbol{\theta}_d = \boldsymbol{\theta}_1 - \boldsymbol{\theta}_2$. In the near field the photon pairs are

close to each other which means in the far field they should have exactly opposite positions. We thus expect to have a coincidence image with large structures. Mathematically we can derive this from the fact that the function g_{spike} of the difference coordinate (defined in Equation (36)) is much broader than f_{spike} of the summed coordinate (Equation (35)).

Figure 12 depicts the results of a difference coordinates scan. We centered the scan at a bright speckle. We find that in the difference coordinates scan we continue to look at the same speckle over a large angle. The size of this angle depends on the opening angle of the diffuser and the angle of the SPDC illumination. We estimated the spread by fitting the autocorrelation function. We found a width of 8.0 mrad by 7.6 mrad. Equation (36) relates the size of the speckle in difference coordinates to w_-. Please note our measurement consists of only a single speckle and therefore the results are rather imprecise. If we disregard this remark and use the average angular spread we obtain $w_- = 2\lambda_0/2\pi 7.8$ mrad $= 34$ μm.[11] This value is large as compared to the value $w_- = 18$ μm obtained from Equation (25), but comparable to values of 22 μm and 32 μm found for the width (FWHM) of the fine structure in the biphoton field by H.D. Lorenzo Pires.

7.4 Reduction of spatial modes

In our final experiment we used an aperture to spatially truncate the incoming SPDC beam. The diameter of the aperture is $d_a = 1.5$ mm. The aperture is placed in Far Field 1 of Figure 8 and care is taken to center the aperture onto the beam. The aperture reduces the number of the spatial modes in the SPDC light. The full far field angle of the aperture is $\theta_a = d_a/f = 7.5$ mrad, where $f = 250$ mm is the focal distance of lens C from Figure 8. The opening angle of the SPDC beam is $\theta_{\text{SPDC}} = \frac{\lambda_0}{\pi w_-} = 14.6$ mrad. The truncation is expected to approximately reduce the number of modes by a factor $(\theta_a/\theta_{\text{SPDC}})^2 = 0.26$.

We scanned the difference coordinates and expect the structures to be smaller because the lesser modes disable the system to keep the speckle picture constant over a large region of the difference coordinate. The results are given in Figure 13. Using a fit of the spike of the autocorrelation (not shown) we now estimate that the structures are 2.1 mrad by 1.8 mrad. There is a large uncertainty in this estimate because the contrast in the difference scan was not very high. Equation (36) relates the size of the speckle in difference coordinates to w_-. From the average width of the spike we estimate that

[11] The extra factor 2 in the denominator compared to Equation (36) represents that the width was estimated in single detector coordinates while the formula is expressed in difference coordinates

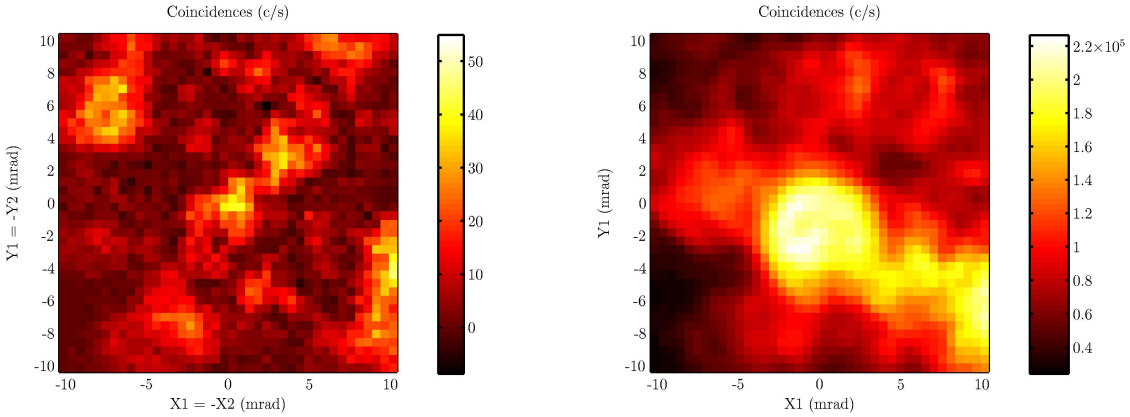

Figure 13: Behavior of the diffuser for spatially truncated SPDC light. On the left are coincidence counts observed in a difference coordinates scan. On the right are the single photon counts versus detector positions. Some intensity speckle can be observed.

$w_- = 2\lambda_0/2\pi 2.0$ mrad $= 131$ μm.[12] From Equation (27) and the measured size of the pump spot w_p the implied number of modes is only $N_m = 1.6$.

In the single photon counts there is now evidence of speckle. The contrast in the biphoton speckle is $C = 1.1$. But when the SPDC light is truncated also the single photon speckle is observed. The contrast defined by Equation (16) in the single photon speckle is $C = 0.46$, which is high compared to the contrast $C = 0.08$ of the speckles in non-truncated SPDC light. The width of the speckles is 2.4 mrad, large compared to the average size of speckles we expect from the pump. However this result may be due to statistical fluctuations in speckle size.

[12]The extra factor 2 in the denominator represents that the width was estimated in single detector coordinates while the formula is expressed in difference coordinates

Experiment	Figure	Parameter	
		w_p (μm)	w_- (μm)
Direct measurement		170	18
Single fixed 1	9 (upper left)	263	
Single fixed 2	10 (upper left)	125	
Single fixed second detector 1	10 (upper right)	125	
Single fixed 3	11 (top)	154	
Parallel scan	11 (middle)	131	
Parallel scan zoomed	11(bottom)	154	
Anti parallel scan	12 (left hand side)		34

Table 3: Summary of the parameters w_p and w_- of the biphoton field estimated from the various biphoton speckles and their directly measured values.

8 Conclusion

We measured both classical intensity speckle and biphoton coincidence speckle. Our classical measurements concerned the far field and near field for three diffusers. Diffuser 1 with an opening angle of $0.5°$, diffuser 2 also with an opening angle of $0.5°$ and diffuser 3 with an opening angle of $1°$.

Using the average intensity in the far field and plots of the average autocorrelation we found that none of the diffusers has a circular scattering distribution. All the diffusers are anisotropic scatterers with an elliptical distribution in the far field.

We found that diffuser 1 is strongly birefringent. There is also a large variation in this birefringence angle. We found that the orientation of the fast and slow axis are constant over the surface of the diffuser. Diffuser 3 also exhibits birefringence but to a lesser degree. There is no measurable variation in this angle. Also for this diffuser the fast and slow axis are constant over the diffuser.

For the quantum experiment we illuminated diffuser 3 with (a near field image of) entangled photon pairs generated in spontaneous parametric downcoversion (SPDC). We scanned one detector, keeping the other detector fixed to find the first biphoton speckle. We found that if we scanned using the other detector, keeping the first detector fixed, we obtained nearly the same speckle pattern. The size of the individual speckles depends on the width of the crystal image on the diffuser.

We linked the first and second detector to make their displacements parallel. Thus we scanned keeping the distance between the detectors constant and measured a speckle pattern that was identical to the speckle pattern measured with one fixed scanner at a double resolution.

Another approach was a scan where the detectors are moving antiparallel. This way the average position of the detectors was kept constant. This speckle pattern contained very large structures. The width of these structures was related to average distance between the photons of an entangled pair.

Reducing the dimensionality of the entanglement results in reappearance of the classical speckle. It also changes the size of the structures in the scan with antiparallel moving detectors. This is because there are too few spatial SPDC modes available in relation to the scattering channels based on the diffuser and pump size.

9 Further research

Biphoton speckles are a fascinating subject and offer lots of opportunities for further research. We will mention four.

First we think it is interesting to take a closer look at the dependence on the number of modes of the SPDC beam and the number of scattering channels of the diffuser.

We can also think of alternative ways to generate biphoton speckles. For can for instance illuminate the diffuser plate with the far field of the SPDC beam. The photon pairs we offer now have a very different spatial correlation structure. It would be interesting to see the effects on the biphoton speckle.

A third interesting subject for further research is the information that biphoton speckle contain about the scattering medium. Are biphoton speckle more informative than the classical speckle? Is it possible to tell the difference between a random phase plate and a bulky scattering medium by looking at their biphoton speckle patterns?

The fourth suggestion is based on the discrepancies between theoretical and measured values of parameters in our research. In the analysis of our results on biphoton speckle we found large variation in the measured speckle width between the different experiments. We tentatively attribute these fluctuations to statistical variations in the speckle pattern that results from the small number of speckles. It would be interesting to test this proposition using numerical simulation.

A Intensity distributions

We define Ψ_i the complex amplitudes at $i = 1..N$ positions. Now we define $\mathbf{\Psi} = (\Psi_1 - \langle\Psi_1\rangle, \Psi_2 - \langle\Psi_2\rangle, ...\Psi_N - \langle\Psi_N\rangle)$. The probability to find a certain configuration $\mathbf{\Psi}$ is

$$P(\mathbf{\Psi}) = \frac{1}{\pi^N \det C} \exp\left(-\mathbf{\Psi}^{*T} C^{-1} \mathbf{\Psi}\right) \tag{39}$$

Where $C = \langle \mathbf{\Psi}^{*T} \mathbf{\Psi} \rangle$, now using $N = 1$ and the fact that in one dimension $\langle \mathbf{\Psi}^{*T} \mathbf{\Psi} \rangle = \langle I \rangle$ gives

$$P(\mathbf{\Psi}) = \frac{1}{\pi \langle I \rangle} \exp\left(\frac{-|\Psi_1 - \langle\Psi_1\rangle|^2}{\langle I \rangle}\right) \tag{40}$$

Now we rewrite this complex Gaussian to a real Gaussian distribution using the polar coordinates $\mathbf{\Psi} = Ae^{i\phi}$, where A and ϕ are real numbers. The Jacobian of this transformation is

$$J = \begin{vmatrix} \frac{\partial \mathrm{Re}(\Psi)}{\partial A} & \frac{\partial \mathrm{Im}(\Psi)}{\partial A} \\ \frac{\partial \mathrm{Re}(\Psi)}{\partial \phi} & \frac{\partial \mathrm{Im}(\Psi)}{\partial \phi} \end{vmatrix} = |\cos(\phi) iA\cos(\phi) - i\sin(\phi)(-A\sin(\phi))| = |iA| = A \tag{41}$$

Now

$$P(A, \phi) = P(\Psi)|J| = \frac{A}{\pi \langle I \rangle} \exp\left(\frac{-A^2}{\langle I \rangle}\right) \tag{42}$$

Integrating over ϕ

$$P(A) = \int_0^{2\pi} \frac{A}{\pi \langle I \rangle} \exp\left(\frac{-A^2}{\langle I \rangle}\right) d\phi = \frac{2A}{\langle I \rangle} \exp\left(\frac{-A^2}{\langle I \rangle}\right) \tag{43}$$

Substituting $I = A^2$ yields the final result

$$P(I) = P(A)\frac{\partial A}{\partial I} = P(A)\frac{1}{2A} = \frac{1}{\langle I \rangle} \exp\left(\frac{-I}{\langle I \rangle}\right) \tag{44}$$

This is the Rayleigh distribution which is generally true for intensities that are the result of a random process.

B Derivation of Gaussian Schell model

This appendix aims to derive the results for the correlation and average intensity functions, from the most fundamental assumptions in the Gaussian Schell model. For notational ease we will not explicitly write the factors in front of the exponentials.

The equations are worked out only for the coordinate x rather than x, y. The generalization to two dimensions is fairly straightforward using the vector notation used in chapter 2. Assume that the pump beam falls in perpendicular to a phase plate.

We assume that the incoming beam has a Gaussian profile. That is the complex electric field at position x (perpendicular to the direction of the beam) has magnitude

$$E_{\text{in}}(x) = e^{-\frac{x^2}{w_p^2}}. \tag{45}$$

The diffuser will add a random phase $\phi(x)$, dependent on the transverse position x, to the incident field. Neglecting the average thickness of the plate, the outgoing electric field is

$$E_{\text{out}}(x) = E_{\text{in}}(x)e^{i\phi(x)}. \tag{46}$$

The far field is given by the Fourier transform of the near field:

$$\widetilde{E}_{\text{out}}(q) = \int e^{iqx} E_{\text{out}}(x)dx. \tag{47}$$

Its average autocorrelation function in the far field is defined by

$$\begin{aligned} \Gamma^{(1)}(q_1, q_2) &= \left\langle \widetilde{E}_{\text{out}}(q_1)\widetilde{E}^*{}_{\text{out}}(q_2) \right\rangle \\ &= \int e^{i(q_1x_1 - q_2x_2)} e^{-\frac{x_1^2+x_2^2}{w_p^2}} \left\langle e^{i(\phi(x_1)-\phi(x_2))} \right\rangle dx_1 dx_2 \end{aligned}$$

where $\langle\cdot\rangle$ is an ensemble mean over al the possible positions of the diffuser. Now we assume that the $\phi(x)$ has a Gaussian distribution for any value of x. Then also $\Delta\phi(x_1, x_2) = \phi(x_1) - \phi(x_2)$ has a Gaussian distribution and it holds that

$$\langle \exp\left[i\Delta\phi(x_1, x_2)\right]\rangle = \exp\left[\left\langle -\frac{1}{2}\left(\Delta\phi(x_1, x_2)\right)^2 \right\rangle\right]. \tag{48}$$

Because for a Gaussian distribution for $\Delta\phi$ with width $\Delta\phi_0$

$$\begin{aligned}
\langle \exp(i\Delta\phi) \rangle &= \int_{-\infty}^{\infty} \exp(i\Delta\phi) \exp\left(-\frac{\Delta\phi^2}{\Delta\phi_0^2}\right) d\Delta\phi && (49)\\
&= \int_{-\infty}^{\infty} \exp\left(-\frac{\Delta\phi_0^2}{4}\right) \exp\left(-\frac{(\Delta\phi^2 - i/2\Delta\phi_0^2)}{\Delta\phi_0^2}\right) d\Delta\phi && (50)\\
&= \exp\left(-\frac{\Delta\phi_0^2}{4}\right) && (51)\\
\left\langle (\Delta\phi^2) \right\rangle &= \int_{-\infty}^{\infty} (\Delta\phi^2) \exp\left(-\frac{\Delta\phi^2}{\Delta\phi_0^2}\right) d\Delta\phi && (52)\\
&= \exp\left(-\frac{\Delta\phi_0^2}{4}\right) && (53)
\end{aligned}$$

If the Gaussian assumption does not hold the equation is only true up to the first two terms of the Taylor expansion.

$$\begin{aligned}
\langle \exp\left[i\Delta\phi(x_1, x_2)\right] \rangle &= 1 - \frac{1}{2}\left\langle (\Delta\phi(x_1, x_2, \zeta))^2 \right\rangle + \\
&\quad \frac{1}{24}\left\langle [\Delta\phi(x_1, x_2)]^4 \right\rangle + ... \\
\exp\left[\left\langle -\frac{1}{2}\left(\Delta\phi(x_1, x_2)\right)^2 \right\rangle\right] &= 1 - \frac{1}{2}\left\langle (\Delta\phi(x_1, x_2))^2 \right\rangle + \\
&\quad \frac{1}{8}\left\langle (\Delta\phi(x_1, x_2))^2 \right\rangle^2 + ...
\end{aligned}$$

Using $\langle \Delta\phi(x_1, x_2)^2 \rangle = (x_1 - x_2)^2/2w_1$ we can simplify the expression for the autocorrelation. This is a crucial assumption in the Gaussian Schell model. We substitute the x_1 and x_2 variables for their sum and difference.

$$\begin{aligned}
u_1 &= x_1 + x_2 \\
u_2 &= x_1 - x_2
\end{aligned}$$

The equation for the unscaled autocorrelation becomes

$$\begin{aligned}
\Gamma^{(1)}(q_1, q_2) &= \left\langle \widetilde{E}_{\text{out}}(q_1) \widetilde{E}^*{}_{\text{out}}(q_2) \right\rangle \\
&= \int e^{\frac{i}{2}(u_1(q_1 - q_2) + u_2(q_1 + q_2))} e^{-\frac{u_1^2 + u_2^2}{2w_p^2}} e^{\frac{u_2^2}{2w_1^2}} du_1 du_2
\end{aligned}$$

This can be factored and computed

$$\Gamma^{(1)}(q_1, q_2) = \exp\left(-\frac{w_p^2}{2}(q_1 - q_2)^2\right) \exp\left(-\frac{1}{2\left(w_p^{-2} + w_1^{-2}\right)}(q_1 + q_2)^2\right) \tag{54}$$

The average intensity in the far field is equal to the autocorrelation of this field at $q_1 = q_2 = q$. Filling this in yields

$$\left\langle \widetilde{I}(q) \right\rangle = \exp\left(-2\left(w_p^{-2} + w_1^{-2}\right)^{-1} q^2\right) \tag{55}$$

The autocorrelation of the electric field is the autocorrelation scaled with the intensity. We can approximate the geometric mean of two intensities with the intensity in the point between. This approximation will be correct if there is not too much change in the intensity between two points. Now we find that the autocorrelation solely depends on the difference between q_1 and q_2

$$\begin{aligned} g^{(1)}(q_1, q_2) &= \frac{\Gamma^{(1)}(q_1, q_2)}{\sqrt{\left\langle \widetilde{I}(q_1) \right\rangle}\sqrt{\left\langle \widetilde{I}(q_2) \right\rangle}} \\ &\approx \frac{\Gamma^{(1)}(q_1, q_2)}{\left\langle \widetilde{I}(\frac{q_1+q_2}{2}) \right\rangle} \\ &= \exp\left(-\frac{w_p^2}{2}(q_1 - q_2)^2\right) \end{aligned}$$

Now we are ready to compute the autocorrelation in intensities $\Gamma^{(2)}(q_1, q_2) = \left\langle \widetilde{I}(q_1)\widetilde{I}(q_2) \right\rangle$. From the complex Gaussian moment theorem we find that

$$g^{(2)} = 1 + \left|g^{(1)}\right|^2 \tag{56}$$

Now $\Gamma^{(2)}$ depends straightforwardly on $g^{(2)}$

$$\begin{aligned}
\Gamma^{(2)}(q_1,q_2) &= \left\langle \widetilde{I}(q_1)\right\rangle \left\langle \widetilde{I}(q_2)\right\rangle g^{(2)} \\
&= \left\langle \widetilde{I}(q_1)\right\rangle \left\langle \widetilde{I}(q_2)\right\rangle \left(1+\left|\frac{\Gamma^{(1)}(q_1,q_2)}{\sqrt{\left\langle \widetilde{I}(q_1)\right\rangle}\sqrt{\left\langle \widetilde{I}(q_2)\right\rangle}}\right|^2\right) \\
&= \exp\left(-2\left(w_p^{-2}+w_1^{-2}\right)^{-1}\left(q_1^2+q_2^2\right)\right)+ \\
&+ \exp\left(-\frac{w_p^2}{2}\left(q_1-q_2\right)^2\right)\exp\left(-\frac{1}{2\left(w_p^{-2}+w_1^{-2}\right)}\left(q_1+q_2\right)^2\right) \\
&= \exp\left(\frac{-\left(q_1-q_2\right)^2-\left(q_1+q_2\right)^2}{\left(w_p^{-2}+w_1^{-2}\right)}\right)\left[1+\exp\left(-\left(1+\frac{w_p^2}{w_1^2}\right)\left(q_1-q_2\right)^2\right)\right]
\end{aligned}$$

When the width of the beam is large compared to the structures on the diffuser plate, $w_p >> w_1$ then the formula can be simplified to

$$\Gamma^{(2)}(q_1,q_2)=\exp\left(-w_1^2\left(q_1+q_2\right)^2\right)\left[\exp\left(-w_1^2\left(q_1-q_2\right)^2\right)+\exp\left(-w_p^2\left(q_1-q_2\right)^2\right)\right] \tag{57}$$

The information in the function is contained by w_p and w_1 and we loose little by integrating out the dependence on q_1+q_2.

$$\begin{aligned}
\Gamma^{(2)}(\Delta q) &= \int_{-\infty}^{\infty}\Gamma^{(2)}(q_1,q_2)d(q_1+q_2) \\
&= \exp\left(-w_1^2\left(\Delta q\right)^2\right)+\exp\left(-w_p^2\left(\Delta q\right)^2\right)
\end{aligned}$$

Rewriting the equation in Δq to $\Delta\theta$ using

$$\Delta q=\frac{\lambda\Delta q}{2\pi} \tag{58}$$

yields equation (9) in chapter 2.

C Computation of the correlation function

The function we like to compute is $\Gamma^{(2)}(q_1, q_2) = \left\langle \widetilde{I}(q_1)\widetilde{I}(q_2) \right\rangle$. In practice we work in two dimensions, so evaluating this function directly would have four components $q_{x1}, q_{x2}, q_{y1}, q_{y2}$ so computing the covariance in computationally infeasible.

The first simplification we make is to only look at the difference coordinates Δq. Second we compute the covariances from single pictures using

$$\widehat{\Gamma}^{(2)}(\Delta q) = \int_{-\infty}^{\infty} I(q' + \Delta q/2) I^*(q' - \Delta q/2) dq' \tag{59}$$

We compute this integral using the following Fourier relations

$$\begin{aligned}
\widehat{\Gamma}^{(2)}(\Delta q) &= \int_{-\infty}^{\infty} I(q' + \Delta q/2) I^*(q' - \Delta q/2) dq' \\
&= \int_{-\infty}^{\infty} \int_{-\infty}^{\infty} I(q' + u) I^*(q' - u) \delta(u - \Delta q/2) dq' du \\
&= \int_{-\infty}^{\infty} \int_{-\infty}^{\infty} \int_{-\infty}^{\infty} I(q' + u) I^*(q' - u) e^{ik(u - \Delta q/2)} dq' du dk \\
&= \frac{1}{2} \int_{-\infty}^{\infty} \int_{-\infty}^{\infty} \int_{-\infty}^{\infty} I(x) I^*(y) e^{ik(x - y - \Delta q)/2} dx dy dk \\
&= \int_{-\infty}^{\infty} e^{-ik'\Delta q} \int_{-\infty}^{\infty} e^{ik'x'} I(x) dx \int_{-\infty}^{\infty} I^*(y) e^{-ik'y} dy dk' \\
&= \int_{-\infty}^{\infty} e^{-ik'\Delta q} \left| \int_{-\infty}^{\infty} e^{ik'x'} I(x') dx \right|^2 dk'
\end{aligned}$$

The final formula yields a method to compute the autocorrelation function from an intensity distribution:

1. Compute the Fourier transform of the (two dimensional) intensity distribution.
2. Take the squared absolute value of the (possible complex) Fourier components.
3. Fourier transform the results back to the intensity domain.

D Optical alignment techniques

D.1 Autocollimation

The first technique used to place objects in the focus of a lens is the autocollimation method. The object that will be placed in the focus later is replaced with an autocollimation plate. The back of the plate is lit with a normal lamp, the image of the plate is converged by the lens onto a mirror and then reflected back onto the lens and finally back onto the backside of autocollimation plate (see Figure 14). The position of the autocollimation plate and the lens can be changed until there is a sharp image on the plate. Then the distance between the lens and the plate is exactly equal to the focal distance of the lens. Now we can replace the plate with the object that we want in the focus of the lens.

D.2 USAF plate focussing

If we have the possibility to take pictures of objects that we want in the focus of a lens system, we can first replace the object with a USAF plate. This plate is especially suited to make a sharp image. If the image is optimally sharp the USAF plate is in the focus of the lens and can be replaced with the object.

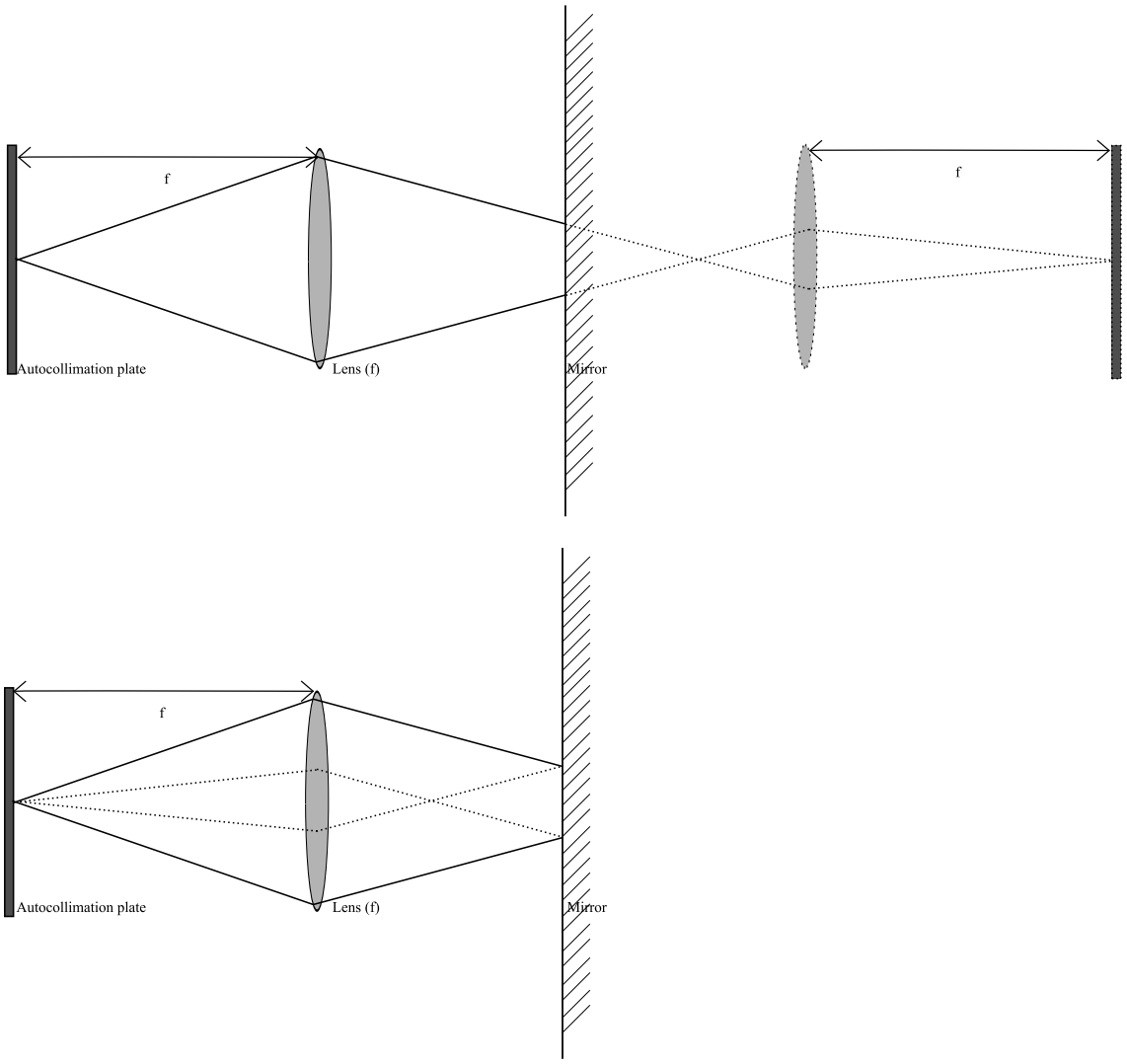

Figure 14: Schematic picture of the autocollimation procedure. The autocollimation plate is a diffuse plate with a periodic structure of holes of which an image can be made. This is the object in the system of a lens and a mirror. The upper picture shows that this setup resembles a telescope with two equal lenses. The lower picture shows a perfect image of the structure will be shown if the distance between the lens and how the plate is exactly equal to the focal distance of the lens. The distance between the lens and the mirror is not relevant.